DOE/JPL-956525-85/05
9950-1181

DRL No. 198
DRD Line Item No. SE-8

DOE/JPL-956525-85/8
Distribution Category UC-63

HEAVY DOPING EFFECTS IN HIGH EFFICIENCY SILICON SOLAR CELLS

Annual Report

For Period Covering
June 24, 1984 - June 23, 1985

By:

F. A. Lindholm and A. Neugroschel
UNIVERSITY OF FLORIDA
Department of Electrical Engineering
Gainesville, FL 32611

JPL Contract No. 956525

The JPL Flat-Plate Solar Array Project is sponsored by the U. S. Department of energy and forms part of the Solar Photovoltaic Conversion Program to initiate a major effort toward the development of low-cost solar arrays. This work was performed for the Jet Propulsion Laboratory, California Institute of Technology, by agreement between NASA and DOE.

This work was performed for the Jet Propulsion Laboratory, California Institute of Technology, and was sponsored by the U. S. Department of Energy through an agreement with the National Aeronautic and Space Administration.

TABLE OF CONTENTS

SUMMARY (EXTENDED ABSTRACT)

We report the first use of a (silicon)/(heavily doped polysilicon)/(metal) structure to replace the conventional high-low junction (or back-surface-field, BSF) structure of silicon solar cells. Compared with BSF and back-ohmic-contact control samples, the polysilicon-back solar cells show improvements in red spectral response and open-circuit voltage. Measurement reveals that a decrease in effective surface recombination velocity S is responsible for this improvement. Decreased S results for n-type (Si:As) polysilicon, consistent with past findings for bipolar transistors, and for p-type (Si:B) polysilicon, reported here for the first time. Though the present polysilicon-back solar cells are far from optimal, the results suggest a new class of designs for high efficiency silicon solar cells. Detailed technical reasons are advanced to support this view.

We present the results of an experimental study designed to explore both qualitatively and quantitatively the mechanism of the improved current gain in bipolar transistors with polysilicon emitter contact. Polysilicon contacts were deposited and annealed at different conditions. The electrical properties were measured using p/n junction test structures that are much more sensitive to the contact properties than are bipolar transistors. A simple phenomenological model was used to correlate the structural properties with electrical measurements. Possible transport mechanisms are examined and conjectures are made about upper bounds on transport parameters in the principle regions of the devices. The main conclusion of this study is that the minority carrier transport in the polycrystalline silicon is dominated by a highly disordered layer at the polysilicon-monosilicon interface characterized by very low minority-carrier mobility. The effective recombination velocity at the n^+ polysilicon - n^+ monosilicon interface was

found to be a strong function of fabrication conditions. The results indicate that the recombination velocity can be much smaller than 10^4 cm/sec.

The decay of excess carriers induced in a semiconductor sample by a laser pulse is studied. The decay rate is proved to be independent of the spatial dependence of the hole-electron generation rate provoked by the laser beam. The effect of surface recombination can be minimized by waiting until the response drops to about one-percent of its initial value. The accuracy of photoluminescence decay measurements of Auger lifetime is examined in view of this and other criteria developed here.

The activation behavior of the minority-carrier mobility and diffusivity in heavily doped ($\sim 10^{20}$ cm^{-3}) Si (Si:As) is investigated in the temperature range, 20 K to 350 K. Experimental results indicate that hole transitions between the valence band and localized shallow states give rise to the observed behavior. The activation energy is about 10 meV, which suggests that the localized states originate from band tails but does not rule out trapping at boron atoms in the compensated n^+ region.

Photoconductive decay provides a method for estimating recombination lifetime in semiconductors. It often exhibits a single characteristic time. For samples having large recombination-center densities, previous experiments indicate that this characteristic time can considerably exceed the steady-state lifetime. We present apparently the first explanation of these results. The explanation involves the effect on the overall photoconductive decay of the multiple characteristic times that describe trapping and recombination through bound states for variations of the electrochemical potentials that are small relative to the thermal voltage.

A reciprocity theorem is presented that relates the short circuit current of a device, induced by a carrier generation source, to the minority carrier

Fermi level in the dark. The basic relation is general under low injection. It holds for three dimensional devices with position dependent parameters (energy gap, electron affinity, mobility, etc.), and for transient or steady-state conditions. This theorem allows calculation of the internal quantum efficiency of a solar cell by using the analysis of the device in the dark. Other applications could involve measurements of various device parameters, interfacial surface recombination velocity at a polycrystalline silicon emitter contact, for example, by using steady-state or transient photon or mass-particle radiation.

A new method for accurate measurement of minority-carrier diffusion coefficients in silicon is described. The method is based on a direct measurement of the minority-carrier transit time through a narrow region of the p-n junction diode. The minority-carrier mobility is obtained from the diffusion coefficient using the Einstein relation. The method is demonstrated on low-doped n- and -p-type Si (dopings $\sim 10^{15}$ cm^{-3}) and is compared with the literature data for the majority-carrier mobilities. The results show that in low-doped Si the electron minority- and -majority-carrier mobilities are comparable, but the hole minority-carrier mobility is significantly higher ($\sim$ 30%) than the corresponding majority-carrier value. The results confirm earlier data of Dziewior and Silber.

CHAPTER ONE
INTRODUCTION

This annual report describes technical findings resulting from JPL contract 956525 for the period June 24, 1984 to June 23, 1985.

The purpose of this contract is to assess the status of critical parameters describing heavily doped silicon, to integrate this assessment into an effort aiming toward determination of these parameters and their incorporation in silicon solar cell design, and to develop associated measurement methods. The interest in heavily doped silicon extends to heavily doped polysilicon, particularly to its use as a quasi-blocking contact at surfaces. It extends also to measurement methods designed to explore dilutely doped silicon, which typically adjoins heavily doped layers in silicon solar cells.

Professors Fred A. Lindholm and Arnost Neugroschel of the Electrical Engineering Department of the University of Florida serve as principal investigators for this contract. Several graduate students have participated significantly in the conduct of the research: T. W. Jung, J. J. Liou, K. Misiakos, and J. S. Park. Other collaborators have included Peter Iles, M. Arienzo, B. Y. Hwang, Y. Komen, R. Issacson, M. Spitzer and Professors P. T. Landsberg and C. T. Sah.

In the brief description to follow presently concerning the content of the chapters of this report, some of these people named above are indicated, through the appearance of their initials, as principal contributors to the chapter being described.

Prior to outlining the content of each chapter, we list immediately below the journal papers (two invited) and the conference papers (including one invited plenary lecture) that have resulted from this contract research. Only those papers for the present reporting period, June 1984 to June 1985, are

listed. We include both papers published and papers accepted during this period.

PAPERS SUPPORTED BY CONTRACT #956525

F. A. Lindholm and J. J. Liou, "Improved determination of lifetime and surface recombination velocity by observing transient voltages," 18th IEEE Photovoltaic Specialists Conference, October 1985 (invited plenary lecture to be presented).

F. A. Lindholm, A. Neugroschel, M. Arienzo, and P. A. Iles, "Front and back polysilicon-contacted solar cells," 18th IEEE Photovoltaic Specialists Conference, October 1985.

K. Misiakos and F. A. Lindholm, "Generalized reciprocity theorem for semiconductor devices," J. Appl. Phys., tentatively scheduled for October 1, 1985.

K. Misiakos and F. A. Lindholm, "Toward a systematic design theory for silicon solar cells using optimization techniques", Solar Cells, Oct. 1985 (invited paper).

A. Neugroschel, F. A. Lindholm, and C. T. Sah, "Trap controlled minority-carrier mobility in heavily doped silicon," Solar Cells, to appear in Sept. 1985.

A. Neugroschel, "Minority-carrier diffusion coefficients and mobilities in silicon," IEEE Electron Device Letters, vol. EDL-6, pp. 425-427, August 1985.

K. Misiakos, F. A. Lindholm, and A. Neugroschel, "Solution of the continuity equation in planar symetry cases and assessment of photoluminescence decay," J. Applied Physics, vol. 58, pp. 1647-1650, August 1985.

F. A. Lindholm, A. Neugroschel, M. Arienzo, and P. A. Iles, "Heavily doped polysilicon contact solar cells," IEEE Electron Device Letters, vol. EDL-6, pp. 363-365, July 1985.

P. T. Landsberg, A. Neugroschel, F. A. Lindholm, and C. T. Sah, "A model for band-gap shrinkage in semiconductors with application to silicon," Physica Status Solidi (a), to be published July 1985.

F. A. Lindholm, "Uncertainties about the physical electronics of n^+ and p^+ silicon, with applications for solar cells", Solar Cells, vol. 12, pp. 131-140, June-July 1984 (invited paper).

B. Y. Hwang and F. A. Lindholm, "Detailed interpretation of photoconductivity decay response for lifetime determination," Solar Cells, vol. 14, No. 2, pp. 187-190, May 1985.

A. Neugroschel, M. Arienzo, Y. Komen, and R. D. Isaac, "Experimental study of the minority carrier transport at the polysilicon monosilicon interface," IEEE Trans. Electron Devices, vol. ED-32, pp. 807-816, April.

O. von Roos and F. A. Lindholm, "Steady state currents in semiconductor filaments or grains in case of large surface recombination velocity on lateral surfaces," J. Appl. Phys., vol. 57, pp. 415-417, January 1985.

This report proceeds as follows. Chapter Two (FL, AN, MA, PI) describes the first use of polycrystalline silicon as a passivant for the surfaces of silicon solar cells. Chapter Three (AN, MA, YK, RI) reports experimental findings about the mechanisms underlying this passivation--that is, this reduction of surface recombination velocity. For doping concentrations of about $10^{16}/cm^3$, we inferred that the value of this velocity could be as small as 15 cm/s for small-area devices. Chapter Four (KM, FL, AN) provides a detailed mathematical assessment of the Auger-impact rate coefficients determined by the photoluminescent decay method (Dziewior and Schmid, 1977). We conclude that in principle the method can yield accurate values despite the presence of large surface recombination velocity and despite areal inhomogeneity of the incident laser beam. Chapter Five (AN, FL, CS) examines experimentally the credibility of the model for values of the minority-carrier mobility and diffusivity that are much smaller than the values of the majority carrier counterparts, at least for doping concentrations substantively above $10^{18}/cm^3$. This model involved trapping of minority carrier at bandtail or other shallow bound states associated with the minority-carrier band (Neugroschel and Lindholm, 1983). The results support this model. Chapter Six (BH, FL) provides a detailed interpretation of the photoconductive decay method for examining volume or bulk lifetime in silicon wafers. Chapter Seven (KM, FL) puts forward a generalized reciprocity theorem for semiconductor devices. This theorem allows calculation of the internal

quantum efficiency of a solar cell by using the analysis of the device in the dark. Chapter Eight (AN) sets forth experimental findings concerning the measurements of minority-carrier mobility and diffusion coefficient in dilutely doped silicon (about $10^{15}/cm^3$). The results show that the hole minority-carrier mobility is 30% higher than the majority-carrier value. Design considerations immediately follow from these findings. Chapter Nine briefly discusses the results of this annual report.

CHAPTER TWO
HEAVILY DOPED POLYSILICON-CONTACT SOLAR CELLS

INTRODUCTION

Highly conducting polysilicon contacts to crystalline silicon are widely used in bipolar integrated circuits [1]. Among other properties, these heterojunctions reduce recombination current by forming quasi-blocking contacts [2].

Our purpose is to describe experimental results and their implications deriving from the first use of such contacts in silicon solar cells. Specifically, in this paper we report the results of introducing such contacts at the back surface. The resulting solar cells show large improvements in red spectral response RSR and moderate improvements in open-circuit voltage V_{oc} when compared with control cells made with the conventional back-surface-field (BSF) structure or with back-ohmic contact (BOC) structures. To assess the origin of these improvements, we measure the effective recombination velocity S of minority carriers in the monocrystalline silicon as they enter the polysilicon layer. This determines that S(polysilicon back) < S(BSF controls), and we interpret this lowering of the recombination velocity to be the mechanism responsible for the improvement in V_{oc} and RSR. The solar cells and controls described here have n-type and p-type base regions; the decrease in S resulting from p-type polysilicon (Si:B) is reported here for the first time.

FABRICATION

The substrate resistivity was 2 ± 0.5 Ω-cm for both the p-type and n-type samples. The p-type substrates were chemically polished on the back side; the n-type substrates were polished chemically-mechanically. About 2000 A thick layers of n^+ and p^+ polysilicon was deposited (in-situ doped) at 670°C in an

atomospheric pressure CVD reactor. The n^+-emitter (Si:P) was diffused at 875°C for about 12 min., and the p^+-emitter (Si:B) was diffused at 900°C for 30 min. During the polysilicon deposition and the emitter diffusion, CVD-SiO_2 protected the other side of the sample. Out-diffusion from the doped polysilicon into the base occuring during the emitter diffusion creates a crystalline low-high junction of thickness <200 Å [2]. The thinness of the resulting n^+ (or p^+) layer at the back suggests that negligible recombination occurs in its volume.

The conventional Al-paste alloying technique formed the BSF region to a depth of about 3 to 5 μm for the p-base BSF controls. Phosphorous diffusion formed a one-micron thick BSF region for the n-base BSF controls. These n-base controls and back-ohmic-contact controls had an ohmic contact (Ti + Pd + Ag) deposited and then annealed on the back surface. The p-base samples had a thin layer of Al under the Ti + Pd + Ag, and the heating was below the Al-alloy temperature (~ 400° C).

MEASUREMENTS AND EXPERIMENTAL DATA

We made measurements to compare the merit of the polysilicon-back-contact structure to that of the BSF and BOC controls. Our main object was to explore the influence of the back surface recombination velocity, which enters the boundary-value problem describing the solar cells.

To obtain the boundary-value problem, we follow Shockley in thinking of the device as comprising two quasi-neutral regions separated by a junction space-charge region [3]. We focus on recombination in the volume and at the surface of the quasi-neutral base. If we define the surface as the interface between the silicon and the polysilicon contact, characterized by S, we get a simple model in which the polysilicon recombination and transport mechanisms

are imbedded in S. For a BSF cell, we define the surface as that plane where the low-high (p/p+ or n/n+) crystalline junction begins. Then S characterizes recombination occuring in the transition and heavily doped regions. (The usual carrier density and voltage relations together with the continuity equation for minority carriers, completes the boundary-value problem.)

Using an AMO spectrum, we measured the solar-cell parameters. Of these the one most closely linked to S is the red spectral response RSR, (λ > 6000 A). The data appear in Table 1. For a p-type base, the cells having a polysilicon contact show significant increases in V_{oc} and RSR over those having an ohmic back contact or an aluminum-alloy back surface field. Note, however, that the alloy BSF controls showed no improvement compared with the BOC controls in V_{oc} and only a slight increase in RSR. This indicates that the alloy process failed to yield an effective back-surface field. It is common experience that the alloy process does not consistently yield good BSF regions for ρ as low as 2 Ω-cm, although it is reliable for higher base resistivities. For the cells having an n-type base, both the polysilicon devices and the BSF controls, formed by P diffusion, showed significant and similar increases in RSR when compared with the response of the BOC controls.

To assess whether one can attribute these results to smaller S, we measured S and diffusion length L using an MOS-switch version of the method of Ref. [4]. In these experiments, the silicon-polysilicon junction provides a blocking contact that is markedly superior to the low-high junction of the BSF controls (Table 1).

DISCUSSION AND EXTENSIONS

The most important columns in Table 1 pertain to the red spectral response and to S, which emphasize the improvements deriving from the polysilicon/silicon back contact. The improvement in V_{oc} is less striking, partly because V_{oc} depends not only on S but also on the collective effects of L, shunt conductance and recombination current in the junction space-charge region and in the quasi-neutral emitter.

The polysilicon/silicon junction is also superior in other respects. Process control for BSF devices is critical for good performance. This is particularly true for the Al alloy process commonly used to fabricate a p-type BSF region. As noted, this process does not reliably form good BSF regions for $\rho \lesssim 2$ Ω-cm. For BSF regions formed by solid-state diffusion, the high temperatures required may degrade lifetime and the low-high junction may be shifted by subsequent thermal processing such as that used to form the p/n junction. Both diffusion and alloy processing consumes part of the substrate, which may pose difficulties for thin solar cells. In contrast the polysilicon-back structure derives from a non-critical deposition process at low temperature [2]; the post-deposition heat treatment also is not critical [2]. Polysilicon back processing consumes essentially none of the substrate. It can be controlled precisely and is reliable, as employment in bipolar integrated-circuit technology has shown.

Consider now extensions of the present design. First, consider low-ρ substrates (0.5 Ω-cm < ρ < 0.1 Ω-cm, corresponding to doping concentrations $\sim 10^{17}$ cm^{-3}), which reduce base-region volume recombination, thus tending to increase V_{oc} and efficiency η. However, effective BSF regions on low-ρ substrates have never been made. In BSF solar cells, $Sp \propto \rho^{-1}$ for low-injection conditions [5] and for ρ > 0.5 Ω-cm approximately. For

$\rho < 0.5$ Ω-cm,the potential barrier V(BSF) between the low- ($\sim 10^{17}$ cm^{-3}) and high-doped sides of the BSF junction becomes ineffective: $V(BSF) \simeq (kT/e)\log[N(low)/N_{eff}] < 2.3(kT/e)$ where N(low) is the doping concentration on the low-doped side and $N_{eff} \sim 10^{18}$ cm^{-3} is the <u>effective</u> doping concentration on the high-doped side, corrected for band-gap shrinkage ΔE_G. Thus from Ref. 5, $S = (D/L)\,[N(low)/N_{eff}(high)] \rightarrow D/L = S(max)$, where the minority-carrier diffusivity D and diffusion length L pertain to the highly doped side. For a polysilicon-contacted solar cell, recent experiments [2] show that S_{max}(poly junction) << S_{max}(BSF). The mechanisms underlying the relatively low value of S_{max}(poly junction) are still debated in the literature. The polysilicon of Ref. 2 and that for our devices of Table 1 was deposited without an intentional interfacial oxide, and Ref. 2 advances the view that the low value of S(max) derives from extremely low values of D in the highly disordered interfacial region.

Thus we anticipate that polysilicon deposition can give low-S contacts on base regions having low resistivities (~ 0.1 Ω-cm). From the results of Ref. 2, we anticipate S < 1000 cm/s.

Attaining high efficiency (η) depends on reducing S at the front surface as well. Thermal oxides have proved effective over the surface, exclusive of that portion where ohmic contacts exist. Even though ohmic contacts constitute only 5% or less of the front surface, one should note that the increase in emitter recombination current caused by areal inhomogeneity greatly exceeds that calculated by consideration of the areal ratio of low-S to high-S regions [6,7]. To avoid the resultant drop in η, Green et al. [8] have used thin tunneling oxides between the silicon and the metal. Substitution of heavily doped polysilicon for the tunneling oxides may provide a better contacting structure with higher yield and longer life.

Sah has recently proposed detailed practical designs for controlling the recombination losses at the front, or emitter, surface [9]-[10]. He has proposed using thin and doped polysilicon layers between the metal and the heavily doped silicon surface of the emitter while using a thermal oxide over the emitter area not shadowed by metal. Employing the data of Ref. 2, he has calculated a practical maximum efficiency of above 23% provided by the low recombination losses at the front and back surfaces and assumed volume recombination only by Auger and radiative processes.

Thus, we suggest elements of the following new class of silicon solar cell designs: 1) Use thin ($\simeq$ 150 μm) base regions of resistivity $\sim$ 0.1 Ω-cm contacted on the back by heavily doped polysilicon; 2) Interleave the front surface with oxide and a polysilicon/metal system; 3) Use either an n-type or p-type silicon for the base region.

As suggested by the work of Sah quoted above, we expect that these solar cells could have very high conversion efficiencies. The present work, together with the somewhat related efforts using SIPOS junctions to reduce surface recombination [11], constitute recent significant departures from conventional silicon solar cell designs.

ACKNOWLEDGEMENTS

The portion of this work done at the University of Florida was supported by the Jet Propulsion Laboratory (Contract 956525) and the National Science Foundation (Grant ECS-8203091). We thank T. W. Jung for performing the SCCD measurements.

REFERENCES

1. T. H. Ning and R. D. Isaac, "Effect of emitter contact on current gain of silicon bipolar devices," IEEE Trans. Electron Devices, ED-27, pp. 2051-2055, Nov. 1980.

2. A. Neugroschel, M. Arienzo, Y. Komen, and R. D. Isaac, "Experimental study of the minority-carrier transport at the polysilicon-monosilicon interface," IEEE Trans. Electron Devices, ED-32, pp. 807-816.

3. W. Shockley, "The theory of p-n junctions in semiconductors and p-n junction transistors," Bell Syst. Techn, J., vol. 28, pp. 435-489, July 1949.

4. T. W. Jung, F. A. Lindholm, and A. Neugroschel, "Unifying view of transient responses for determining lifetime and surface recombination velocity in silicon BSF cells, with application to experimental short-circuit current decay," Special Issue on Photovoltaics of the IEEE Trans. Electron Devices, ED-31, pp. 588-595, May 1984.

5. J. R. Hauser and P. M. Dunbar, "Minority carriers reflecting properties of semiconductor high-low junctions," Solid-State Electron., vol. 18, pp. 715-716, July, 1975.

6. F. A. Lindholm, J. A. Mayer, J. R. Davis, and J. I. Arreola, "Degradation of solar cell performance by areal inhomogeneily," Solid-State Electronics, 23, pp. 967-973, Sept. 1981.

7. R. J. Schwartz, J. L. Gray, G. B. Turner, D. Kanani, and H. Ullal, "Numerical modeling of p-i-n hydrogenated thin film silicon solar cells," Proc. of 17th Photovoltaic Specialists Conf., pp. 369-373, May 1984.

8. M. A. Green, A. W. Blakers, J. Shi, E. M. Keller, and S. R. Wenham, "High efficiency silicon solar cells," IEE Trans. Electron Devices, ED-31, pp. 679-683, May 1984.

9. C. Tang Sah, "Barriers to achieving high efficiency," Proceedings of the 23rd Project Integration Meeting, March 14-15, 1984, Progress Report 23, Jet Propulsion Laboratory, pp. 123-130, JPL Publication 84-47.

10. C. Tang Sah, "High efficiency crystalline silicon solar cells," Second technical report, DOE/JPL-056289-84-1.

11. E. Yablonovitch, R. M. Swanson and Y. H. Kwark, "An n-SIPOS: p-SIPOS homojunction and a SIPOS-Si-SIPOS double heterostructure," 17th IEEE Photovoltaic Specialists Conf., pp. 1146-1148, May 1984 (84CH2019-8).

TABLE 1

Summary of measured parameters at 28° C, (no AR coating). The cells have area A = 4 cm^2 and thickness of about 210 ± 10 μm except for cell 2N which was 330 μm thick. The results are the average values from 10-20 cells.

Cell	Base type	Back contact	V_{oc} (mV)	$I_{SCR}(\lambda>0.6\mu m)$ (mA)	L (μm)	S (cm/s)
1P	p	ohmic	573	63	310-350	
2P	p	BSF	574	64	310-350	$4.2x10^4$-$5x10^4$
5P	p	poly-Si BSF	583	67.7	310-350	1100-1500
1N	n	ohmic	566	62.7	190-250	
2N	n	BSF	565	65.2	190-250	700-1000
5N	n	poly-Si BSF	591	65.5	190-250	100-160

CHAPTER THREE
EXPERIMENTAL STUDY OF THE MINORITY CARRIER TRANSPORT AT THE POLYSILICON-MONOSILICON INTERFACE

I. INTRODUCTION

It was demonstrated [1-3] that the common-emitter current gain of bipolar transistors can be improved by replacing the emitter metal contact by a highly doped polysilicon layer. A number of works, both theoretical and experimental, investigating this effect, were published [1-8]. In all these studies, the analysis was done on the actual emitter structure of the bipolar transistor consisting of a thin (~ 2000 A) heavily-doped monocrystalline emitter region contacted by a heavily-doped polysilicon layer about 2000 A thick. The analysis of such a structure is difficult due to uncertainties in the parameters of both the monosilicon and polysilicon bulks and a poor understanding of the interface between the polysilicon and the single crystal silicon layer. These uncertainties are further augmented by the presence of the grain boundaries in the polysilicon. Thus, numerous assumptions are required to establish a minority-carrier transport model in the above system [4-8].

The region which is most difficult to characterize is the polysilicon-monosilicon interface. This region is very sensitive to the fabrication conditions and to the surface treatment before the CVD process of the polysilicon deposition [2,7]. A peak in the arsenic and phosphorus concentration was observed [7,9] as a result of the donor dopant segregation at the interface. The interface may also act as a natural sink for deep-level impurities and cause precipitation of interstitial oxygen from the bulk. The properties of the interface are very strongly influenced by a presence of a very thin insulating interfacial layer created by oxidizing silicon before the polysilicion deposition. This can be achieved by thermal oxidation [2] or by a chemical treatment [7].

These and other variables make the evaluation of the relative importance of the polysilicon bulk and the interface very difficult, both theoretically and experimentally. De Graaf and de Groot [2] investigated the current gain of the $n^+/p/n$ transistors with an intentionally grown oxide layer at the polysilicon-monosilicon interface. They suggested that the current gain enhancement is controlled by the tunneling mechanism through the oxide layer. Ning and Isaac [3] have shown that, for the $n^+/p/n$ transistors with a polysilicon emitter contact with no intentional oxide layer at the polysilicon-monosilicon interface, the minority hole base current becomes a function of polysilicon thickness if the film thickness is less than about 500 Å. This indicates that the current gain enhancement is determined by the hole transport in the polysilcon film within about 500 Å of the interface. The devices used in [3] with different thicknesses of the polysilicon film had identical polysilicon-monosilicon interfaces.

In the present work we have examined the roles of the polysilicon-monosilicon interface and of the polysilicon bulk in much more detail than has been done previously. We intentionally emphasize the interface using devices with identical interface properties, while varying drastically the polysilicon bulk properties. This is achieved by using a bilayer structure of polysilicon films [9], described in detail in the next section. Our approach is, thus, different from that taken by other researchers [2,7] who varied the interface treatment while depositing the same polysilicon layer.

The microstructure of the polysilicon film and of the interface was examined by transmission electron microscopy (TEM) and the distribution of arsenic in the polysilicon film and at the polysilicon-monosilicon interface was studied by means of secondary ion mass spectrometry (SIMS) [9]. These structural properties of the polysilicon film and the interface are correlated, for the first time, with the electrical measurements.

To study the polysilicon-monosilicon interface we use a p/n junction test structure, rather than a bipolar transistor. The test structure and its fabrication are described in Section II. As is discussed later, this structure has a number of important advantages in comparison with the bipolar transistor and will be instrumental in developing the phenomenological transport model and revealing the dominant recombination mechanisms in the polysilicon, Sections III and IV.

II. DESCRIPTION OF DEVICES AND FABRICATION

The test structure, shown in Fig. 1, consists of a 0.06 Ωcm p-type substrate with a thin (~ 0.8 μm) n-type epitaxial layer with doping density $N_{DD} \simeq 10^{16}$ cm^{-3} grown on top. One kind of devices had an n^+ contact ring implanted; the second kind of devices on the same wafer does not have the ring. The purpose of the n^+ ring, which covers less than about 5% of the device area, is to assure a good ohmic contact with the relatively low-doped epitaxial layer. One half of each wafer was contacted by a 1500 Å or 2500 Å thick polysilicon film, Fig. 1(a). The deposition and the heat treatment after the deposition were done very carefully and were specifically designed for the purpose of enabling the separation of the role of the interface and the bulk on the current transport. Wafers were etched in a buffered HF solution prior to polysilicon deposition. It is very important to emphasize here that each kind of polysilicon device had a reference device with a metal Al contact (both with and without the n^+ ring), Fig. 1(b), made on the other half of each wafer. The Al contact was also deposited on top of the polysilicon film. The devices are separated from each other by an oxide layer around the periphery that minimizes the surface leakage, thus assuring that the measured current originates mostly from the bulk. The device areas ranged from 6×10^{-5} cm^2 to 1.2×10^{-2} cm^2.

The polysilicon films, deposited using an atmospheric pressure CVD reactor at 670°C, were one of the following:

(a) 1500 Å undoped polysilicon deposited without any external arsenic source (grain size about 100 Å).

(b) 1500 Å in-situ arsenic doped (grain size larger than about 400 Å).

(c) Bilayer: 1500 Å of undoped film followed by deposition of 1000 Å in-situ doped film (grain size larger than about 300 Å).

Each of these three groups of devices was subjected to various post-deposition treatments. The deposition and annealing conditions are summarized in Table I.

The arsenic-concentration profiles measured by SIMS [9] are shown in Fig. 2 for some of the devices from Table I. These profiles depict the average concentration of the cross section consisting of the grain-boundary region and the bulk. There is evidence [10] that in the in-situ doped films, about 30-50% of the arsenic dopant resides in the grain boundaries. Since the grain boundaries have smaller cross-sectional area than the adjoining grains, the arsenic concentration in the grain boundaries is larger than in the bulk. Based on the diffusion coefficients of arsenic in the polysilicon [9], we infer from the SIMS profiles of the in-situ doped films (Fig. 2.(a)), that the arsenic concentration is about 5×10^{20} cm^{-3} in the grains and about 10^{21} cm^{-3} in the grain boundaries. The dopant in the as-deposited polysilicon film is largely inactive and is subsequently activated during the heat treatment step. The activation ratio (carrier concentration/dopant concentration) depends strongly on the annealing temperature and time [11,12]. For the in-situ doped sample 2BE annealed at 1000°C, 15 min, for example, the activation ratio is about 0.1 [11]. The activation ratio for the devices annealed at 900°C (devices 1C,1D) and at 800°C (device 1B) is not exactly known, but it can be expected to be about 0.01 [11,12].

For the wafers with the bilayer polysilicon film we have employed arsenic diffusion at low temperatures to obtain a preferential grain boundary diffusion from the top in-situ doped layer towards the interface, while minimizing the bulk diffusion [9]. The diffusivity of arsenic in the grain boundaries at T = 800 - 850°C is about three orders of magnitude greater than the diffusivity in the bulk. The SIMS profiles for some of the bilayer samples, before and after the heat treatments, are shown in Fig. 2(b). The arsenic concentration in the originally undoped layer depends upon the heat treatment. As an example, in the bilayer film of the sample 1J after heat treatment at 800°C for 64 hours, arsenic diffused through the grain boundaries and reached the interface [9]. From the SIMS profile, the average arsenic concentration in the grain boundaries is estimated to be about 5 x 10^{20} cm^{-3}. However, in the sample 2BA with a heat treatment at 750°C for 8 hours the arsenic does not reach the polysilicon-monosilicon interface and the arsenic concentration drops from about 10^{21} cm^{-3} in the in-situ doped part of the film to the background concentration of about 10^{17} cm^{-3} - 10^{18} cm^{-3} [9]. This background level is due to the residual impurities in the deposition system and was detected in the undoped film.

Although during the heat treatment arsenic diffuses mainly through the grain boundaries, some diffusion occurs from the grain boundaries to the bulk of the grains. To minimize this outdiffusion, the annealing conditions were tailored in such a way as to allow arsenic to just reach the interface. The outdiffused region is very narrow especially at the interface, where arsenic outdiffuses only during a fraction of the total heat treatment time. For example, for 800°C, 10 hrs, the arsenic concentration should drop from 2 x 10^{20} cm^{-3} to 10^{17} cm^{-3} in about only 100 A. During a fraction of the heat treatment time, arsenic will also diffuse into the epitaxial layer. The width of this diffusion should also be in the order of ~ 100 A. As a result of the

preferential grain boundary diffusion, a heavily doped thin interfacial region ΔW is created at the metallurgical polysilicon-monosilicon interface. Figure 3 illustrates schematically the expected arsenic concentration profiles at the interface corresponding to the SIMS data data for the sample 1J from Fig. 2(b).

Comparison of the SIMS profiles, Figs. 2(a) and 2(b), clearly shows that the in-situ doped and the bilayer devices have similar arsenic, and thus electron, concentrations within about 100-300 A thick interfacial layer ΔW, but their bulk concentrations are different (see Fig. 3). Due to the activation ratio, the in-situ doped devices have a bulk electron concentration of about $N \simeq 5 \times 10^{18} - 5 \times 10^{19}$ cm^{-3} in comparison with $N \ll 10^{18}$ cm^{-3} for the bilayer samples in the originally undoped layer adjacent to the interface. As will be discussed in detail later, separation of the interfacial layer from the rest of the polysilicon film is also necessitated by very different microstructures in these two regions.

Based on this similarity of the polysilicon-monosilicon interfacial layer, if the interfacial layer dominates the minority carrier transport, we expect the in-situ and the bilayer samples exhibit similar electrical properties. If, however, the bulk properties of the polysilicon determine the carrier transport, then we would expect the in-situ doped and the bilayer devices to have different electrical properties.

III. MODEL DEVELOPMENT

In this section we develop a simple phenomenological model for the minority-carrier transport with the aim of identifying the dominant recombination mechanism in the polysilicon-monosilicon structure.

Figure 4(a) shows the test structure under forward bias. For the present purpose we consider the polysilicon-monosilicon interface (Fig. 3) to be a thin layer of width $\Delta W \sim 100$ Å that includes the high-low junction in the epitaxial layer, grain-boundary space-charge-region (SCR) at the metallurgical interface and the highly doped region adjacent to the metallurgical interface in the polysilicon. We assume that this region can be characterized by a single effective time constant $\tau_p(\text{int})$. This assumption simplifies the analysis and will yield useful results.

Using a charge-control representation for the hole current J_p and the electron current J_n at x=0, we write

$$J_p(0) \simeq \frac{Q_p(\text{epi})}{\tau_p(\text{epi})} + \frac{Q_p(\text{int})}{\tau_p(\text{int})} + \frac{Q_p(\text{poly})}{\tau_p(\text{poly})} + J_p(W_E) \tag{1}$$

$$J_n(0) = \frac{Q_n(\text{sub})}{\tau_n(\text{sub})} \tag{2}$$

$$J = J_p(0) + J_n(0) \tag{3}$$

where $Q_p(\text{epi})$, $Q_p(\text{int})$, $Q_p(\text{poly})$ and $Q_n(\text{sub})$ are the excess charges in the epitaxial layer, the interfacial layer, the polysilicon bulk, and the substrate, respectively with corresponding time constants $\tau_p(\text{epi})$, $\tau_p(\text{int})$, $\tau_p(\text{poly})$ and $\tau_n(\text{sub})$, and $J_p(W_E)$ is the recombination current density at the ohmic contact, $x = W_E$. In (1) - (3) we have neglected the recombination in the p/n junction space-charge region which can be evaluated separately [13], if necessary.

Having described the cross-sectional microstructure and composition of our devices, Figs. 2 and 3, and defined the current components, (1) - (3), we will in the next Section analyze the data in order to: (i) separate the

measured current into components and (ii) identify the parameters that determine the minority carrier transport in the interfacial layer and in the polysilicon film.

IV. EXPERIMENTAL RESULTS AND DISCUSSION

A. Summary of Results

Figure 5 shows the measured current-voltage (I-V) characteristics for some representative devices from Table I. The hole saturation current densities J_{p0} for all devices used in this study are listed in column IV of Table I. The values for J_{p0} were obtained by determining the electron saturation current $J_{n0} \lesssim 2 \times 10^{-13}$ A/cm^2 from the doping density and from the measured diffusion length in the p-type substrate ($L_n \gtrsim 9$ μm) obtained by the X-ray method [14] and then subtracting it from the measured saturation current J_0. I-V characteristics were measured both on devices with and without the n^+ contact rings; the values for J_{p0} were identical, but the devices without the n^+ rings had a larger series resistance R_S (see discussion below). The I-V curves exhibited an ideal $J \propto \exp(qV/kT)$ dependence for at least 3-4 decades of current. Thus no corrections for the non-ideal space-charge-region and surface recombination currents were required. The results reported here were measured on devices with an area of 62 x 23 mil^2 in which the perimeter effects are negligible. Each J_{p0} value in Table I is the average value over at least 20 devices.

The following important observations can be made from Fig. 5:

(a) The current density for the in-situ doped polysilicon devices is about 3 orders of magnitude smaller in comparison with that of the metal contact. This demonstrates the sensitivity of our test structure to the interface conditions and the usefulness of the polysilicon contact in suppressing the current.

(b) The heat treatment after the deposition of the in-situ doped polysilicon film causes almost no changes in the measured current. This is evident from the comparison of the device 1A without any heat treatment with the device 1B heat treated at 800°C, 64 hrs.

(c) The undoped polysilicon film, device 1E, behaves as a surface with large recombination velocity with no improvement in comparison with the reference metal contact.

(d) The bilayer device 1I without heat treatment is identical to the undoped device 1E without heat treatment.

(e) The bilayer device 1J after 800°C, 64 hrs heat treatment, exhibits about the same current density as the in-situ doped device 1B with the same heat treatment.

(f) Devices, without the n^+ contact ring, with undoped film (1E) and bilayer film without heat treatment (1I) have a large series resistance R_S, which is demonstrated by the deviation from the $J \propto \exp(qV/kT)$ dependence at $V \gtrsim 0.3$ volts. The series resistance R_S is greatly reduced for these devices if the measurement is taken on the device with the n^+ contact ring, as illustrated in Fig. 5 for the device 1E.

The above observations (a) - (f) and the results in Table I lead us to the following conclusions:

(1) Large currents measured in all devices with the undoped polysilicon layer contacting the monosilicon layer preclude the possibility of an effective thin interfacial oxide layer [2,7] between the polysilicon and the monosilicon in our devices. It was proposed by de Graaf and de Groot [2] that a 20 - 30 Å thick interfacial oxide

layer represents a tunneling barrier for the minority holes, which suppresses the minority-carrier current in the polysilicon. If such a layer was present in our devices, the hole current would be limited by the tunneling mechanism [2,5,8] through this layer in both the doped and undoped samples. In this work, we did not intentionally grow an interfacial oxide prior to the polysilicon deposition that may produce such a tunneling barrier [2,7].

(2) The polysilicon-monosilicon interface is very sensitive to the arsenic concentration, rather than to the electron concentration. This conclusion is based on the observed insensitivity, discussed in (b) above, of the hole current to the heat treatments of the in-situ doped devices. The electron carrier concentration in the CVD deposited polysilicon is a function of the postdeposition heat treatment [11,12] and increases with the heat treatment temperature. Thus, large differences in the carrier concentrations can be expected before and after the heat treatments [11,12]. On the other hand, the arsenic dopant concentration is almost independent of the heat treatment in the in-situ doped films [9].

The correlation between the arsenic concentration at the interface on the one hand, and the current density and R_S on the other hand, is further demonstrated in Fig. 6 for the devices with bilayer polysilicon films. The comparison of device 1I with no heat treatment with two devices after heat treatment (devices 1J,1L) shows a drastic reduction in the current density. The arsenic concentration at the interface before the heat treatment is the residual $\lesssim 10^{18}$ cm^{-3}, while after the heat treatment the concentration is $\sim 10^{20}$ cm^{-3} (see Fig. 2). Device 1K heat treated

at 900°C for 15 min still gives J_{p0} equal to that of the device 1I. Apparently, the arsenic does not reach the polysilicon-monosilicon interface after the 900°C, 15 min thermal treatment. This is consistent with the recently published values for arsenic diffusivity in the grain boundaries [9]. From Fig. 3 in [9] we can deduce that the product $(Dt)^{1/2}$, which is a measure of arsenic penetration through the grain boundaries, has to be much larger than about 500 Å for arsenic to penetrate through the ~ 1500 Å of the originally undoped layer of the bilayer film. For 900°C, 15 min heat treatment, the value of $(Dt)^{1/2}$ is only about 550 Å, but is about 2000 Å for the devices 1J and 1L, where arsenic did reach the interface, as Fig. 2(b) illustrates. The device 2BA, for which $(Dt)^{1/2} \simeq 280$ Å, behaves similarly to device 1K (see Table I). The R_S is large for the non heat treated case and decreases with increasing $(Dt)^{1/2}$, thus directly reflecting the penetration of the highly doped and conductive arsenic front through the grain boundries towards the interface [9]. A large R_S in all undoped devices ($\lesssim 10^{18}$ As/cm^3) and in the bilayer device 1I suggests that the residual arsenic in the undoped films is present mostly in the nonactivating lattice sites, or more probably, that most of the free electrons are trapped at the grain boundaries leaving the grains essentially depleted [15,16], which results in a large resistivity of the polysilicon film. The reduction in R_S after the heat treatment can also be attributed to the lowering of the grain boundary barriers in the polysilicon film because of the increased doping in the vicinity of the grain boundaries [16,17].

B. Separation of Current Components

In the previous discussion we described the electric behavior of devices with various polysilicon films and their correlation with the microstructural composition. Below, we analyze the data and attempt to identify the possible dominant physical mechanisms governing the minority carrier transport in the polysilicon film. In order to do that, we have to first separate the measured currents into components defined in (1) and (2) and, thus, extract the desired values of the recombination currents in the polysilicon. Then we correlate the phenomenological model with experimental results for polysilicon films with different microstructures.

The five current components in (1) - (2) can be divided into two groups, based on the criteria of the doping density in the particular region. Regions with doping densities smaller than about 10^{18} cm^{-3} are expected to exhibit activation energy corresponding to the energy gap of intrinsic Si, while regions with doping much larger than 10^{18} cm^{-3}, will have smaller activation energies (bandgaps) because of the bandgap narrowing ΔE_G [18]. Considering the above criteria, we can write

$$\frac{Q_p(epi)}{\tau_p(epi)} + \frac{Q_n(sub)}{\tau_n(epi)} \alpha\, e^{-E_{GI}/kT} \tag{4}$$

$$\frac{Q_p(int)}{\tau_p(int)} + \frac{Q_p(poly)}{\tau_p(poly)} + J_p(W_E) \alpha\, e^{-(E_{GI} - \Delta\bar{E}_G)/kT} \tag{5}$$

where E_{GI} is the intrinsic Si bandgap, $\Delta\bar{E}_G$ is the average bandgap narrowing for the entire heavily-doped region, Q_{po} and Q_{no} are the preexponential constants in $Q = Q_o \exp(qV/kT)$, and $J_{po}(W_E)$ is the saturation current density. The activation energy in (5) is thus $E_G = E_{GI} - \Delta\bar{E}_G < E_{GI}$. As discussed earlier, the precise value of the $Q_{no}(sub)/\tau_n(sub)$ component was

already determined independently, thus, only the hole current will be discussed henceforth.

Figure 7 shows the activation plots [18] for representative devices, with undoped, bilayer and in-situ doped polysilicon films. The activation curve for the reference device with metal contact is also shown.

To construct the activation plot, we have to properly account for all temperature dependent parameters in (4) and (5). This is done by plotting [18] $C(J_{PO}/T^m)[\exp(\eta_c)/F_{1/2}(\eta_c)] = \exp[-(E_{GI}(0) - \Delta E_G)/kT] = \exp(-E_G/kT)$ versus 1/T. Here, $E_{GI}(0) = 1.206$ eV is the linearly extrapolated energy gap of intrinsic Si at 0 K, C is a temperature independent constant that involves device parameters (such as geometry, doping, minority-carrier mobility, and minority-carrier lifetime), $\eta_c = (E_{FN} - E_C)/kT$ (see Fig. 4(b)), and $F_{1/2}(\eta_c)$ is the Fermi-Dirac integral of the order of 1/2. In the above expression, m=4 for a transparent region bounded by a surface with very large surface recombination velocity, e.g. metal contact or undoped polysilicon contact, where $J_{PO} \propto [n_i^2(kT/q)\mu_p] \propto T^4$, provided that the minority-carrier mobility μ_p is temperature independent [18]. On the other hand, if the metal contact is replaced by a contact with low surface recombination velocity, then $J_{PO} \propto (n_i^2 W/\tau_p) \propto T^3$ [19], i.e, m=3, provided that the minority-carrier lifetime is temperature independent.

In Fig. 7, we show the activation plot for the in-situ doped device 1B and the bilayer device 1J for which J_{PO} (polysilicon) << J_{PO} (metal); thus, m=3. This yields $E_G \simeq 1.206 \pm 0.03$ eV (i.e. $\Delta E_G \simeq 0 \pm 30$ meV). The assumption of $\tau_p \neq f(T)$ is very reasonable in the narrow temperature range, 300 K < T < 370 K used in Fig. 7. The slope of the activation plot is relatively insensitive to small variations in m. For example, the activation energy for the device 1J for m=3.5 is larger by only about 10 meV compared to

that for m=3. Thus, only a negligible error is caused if τ_p varies slightly with T.

In the case of the devices with metal contact and undoped polysilicon contact films, setting m=4 neglects the temperature variation of the minority-carrier mobility μ_p. The result for m=4 is $E_G \approx 1.146 \pm 0.020$ eV, i.e. $\Delta E_G \approx 60 \pm 20$ meV. Assuming now that the temperature dependence of the minority-carrier hole mobility in the low-doped ($\sim 10^{16} cm^{-3}$) epitaxial layer is the same as the temperature dependence of the majority-carrier hole mobility, which follows $\mu_p \propto T^{-1.8}$ for $300\ K \lesssim T \lesssim 400\ K$ [20], then a correction to the above result is required. This is done in Fig. 7 using $T^4 T^{-1.8} = T^{2.2}$ instead of T^4, yielding $E_G \approx 1.206 \pm 0.025$ eV, i.e. $\Delta E_G \approx 0 \pm 25$ meV.

The activation energies for the other devices from Table I, not displayed in Fig. 7, are equal to the values of the representative devices discussed above.

In contrast, Fig. 7 also illustrates the activation curve corresponding to the hole recombination in the n^+ monosilicon layer obtained from the n^+/p monosilicon junction with uniformly doped transparent 0.15 μm n^+ layer with electron concentration $N \approx 2 \times 10^{19}\ cm^{-3}$. The activation energy for this n^+-monosilicon layer (using m=4) is smaller by about 0.135 eV, $E_G \approx 1.071 \pm 0.025$ eV, in comparison with the value for the epitaxial n-monosilicon obtained from the device with the metal contact. This difference can be interpreted as bandgap narrowing in the n^+-monosilicon region of $\Delta E_G \approx 135$ meV [18].

The activation energy of the reference device with the metal contact is described exactly by (4) (polysilicon is absent here) and the current is due completely to the low-doped epitaxial layer ($J_{po} >> J_{no}$) where $\Delta E_G = 0$. The fact that the result obtained from the activation plot of this device gives

$E_G \simeq E_{GI}(0) = 1.206$ eV within the experimental accuracy of about $\pm$ 0.025 eV establishes a credibility for the activation plots and also provides a value for comparison with the devices with polysilicon contacts.

The hole saturation current density for the devices with polysilicon contact in which $J_{po}(\text{polysilicon}) \ll J_{po}(\text{metal})$, assuming $L_p \gg W_{epi}$ and $S_p \ll D_p/W_{epi}$, can be written as [19,21]

$$J_{po} \simeq \frac{qn_i^2}{N_{DD}} \left[\frac{W_{epi}}{\tau_p(epi)} + S_p\right] \quad . \tag{6}$$

Here S_p is the effective surface recombination velocity at $x = W_{epi}$, resulting from the recombination losses in the polysilicon. The observed activation energy and the fact that $J_{po}(\text{polysilicon}) \ll J_{po}(\text{metal})$ imply $S_p \ll W_{epi}/\tau_p(epi)$. The hole distribution corresponding to this case is schematically depicted in Fig. 4(c). From (6) we then find $\tau_p \simeq 0.6$ μsec and $L_p \simeq 26$ μm.

To corroborate the fact that S_p is negligibly small in our devices and to avoid the uncertainties in the interpretation of the activation plots, we have fabricated the test structures by depositing an in-situ doped polysilicon films on epitaxial layers with different values of W_{epi}: 0.8 μm ($\rho \simeq 0.6$ Ωcm), 8 μm ($\rho \simeq 1.2$ Ωcm), and 12.8 μm ($\rho \simeq 0.6$ Ωcm). The deposition and the heat treatment conditions were identical for all three devices. The heat treatment was done at 900°C for 15 min, and corresponds to that of the device 1D from Table I.

Using (6), we can calculate the values of $S_p + W_{epi}/\tau_p(epi)$ from the measured J_{po} and from the known doping densities. Then a plot of $S_p + W_{epi}/\tau_p(epi)$ versus W_{epi} is expected to yield a straight line, with a slope proportional to $\tau_p(epi) \simeq 0.6$ μsec, assuming that τ_p in the 8 μm and 12.8 μm

epitaxial layers is about equal to that in the 0.8 μm layer deduced above. Since S_p is identical for all devices, an extrapolation to $W_{epi} \to 0$ yields S_p. This plot is shown in Fig. 8, yielding $S_p \sim 15$ cm/sec $\ll W_{epi}/\tau_p(epi)$ for all three devices.

The exact value of S_p is of importance, since it represents the desired recombination losses in the polysilicon, including the losses in the interfacial layer. The approximate value of $S_p \sim 15$ cm/sec deduced above indicates that the recombination losses in the polysilicon film are only about 10% of the measured hole current. The polysilicon-monosilicon interface thus acts as a very efficient barrier for the minority carriers.

Hence

$$\frac{Q_{po}(poly)}{\tau_p(poly)} + \frac{Q_{po}(int)}{\tau_p(int)} \lesssim 10^{-13}\ A/cm^2 \qquad (7)$$

where we have neglected $J_{po}(W_E)$ because it was found experimentally [3] that $L_p(poly) \lesssim 500$ Å, which is much less than the thickness of the polysilicon films used in this work.

C. Discussion

The TEM study revealed that the grains in the in-situ doped polysilicon films after heat treatment at 900°C - 1000°C are essentially columnar and the grain diameter is at least 400 Å and as large as about 1000 Å [22]. The effective hole diffusion length in the heavily-doped polysilicon is $L_p \lesssim 500$ Å [3], i.e., $L_p \lesssim$ grain diameter. Such polysilicon film thus has only a few or no grain boundaries in the direction of the current flow and can be considered to be almost a single crystal n^+ layer separated from the monocrystalline epitaxial layer by only grain boundaries (or an interfacial layer) at the

metallurgical interface. Thus, if the very thin (~200 Å) interfacial layer (Figs. 3, 4) is transparent for the minority holes, then the diffusion hole current in the bulk of the polysilicon film with $N \sim 10^{19}$ cm^{-3} is expected to be about equal to the hole current of the single crystal n^+/p junction of Fig. 7 with $N \simeq 2 \times 10^{19}$ cm^{-3} which is $J_{po} \simeq 4 \times 10^{-12}$ A/cm^2 at 25°C. This value is about one decade larger than the measured J_{po} for the devices with the in-situ doped polysilicon films and at least a factor of 40 larger than the value estimated in (7) for the total recombination losses in the polysilicon film. To explain the discrepancy of about two decades in the current, the effective transport parameters in the polysilicon would have to be markedly different from their monosilicon values.

Modeling of the transport in the polysilicon is complicated by the grain boundaries. As a first approximation, we will treat the polysilicon analogously to the transport in the single crystal Si, as justified above, but with an effective value for the parameters, such as bandgap, mobility, and lifetime, to account for the influence of the grain boundaries. The effective parameters are average parameters for the polysilicon film corresponding to the average grain size. This approach was used before [3,4]. We can then write

$$\frac{Q_p(poly)}{\tau_p(poly)} \simeq \frac{qn_i^2}{N_e(poly)} \frac{D_p(poly)}{L_p(poly)} \exp\left(\frac{qV}{kT}\right) \quad , \tag{8}$$

where $N_e(poly) \simeq 10^{18}$ cm^{-3} is the effective doping [18,23] in the heavily doped polysilicon. In (8), we have used the quasi-equilibrium assumption of an almost flat hole quasi-Fermi level in the epitaxial layer up to the metallurgical interface, Fig. 4(b). This is justified by the fact that $J_{po}(polysilicon) \ll J_{po}(metal)$ and by noting that the recombination losses in

the very thin ($\lesssim$ 200 Å) diffused region in the epitaxial layer can be neglected [19,24]. Note here that, to remove the discrepancy, D_p(poly) would have to be at least 40 times smaller than the single crystal value. This is not a likely possibility in the large grains with $L_p \sim$ grain diameter. To explain the results by lower value of ΔE_G in the polysilicon requires a difference of about 100 meV between the single crystal and polysilicon values. However, the measured activation energies in our devices and in the bipolar transistors [3] do not support this assumption.

For the bilayer devices, we have a more complicated situation. The interfacial region is heavily doped, followed by a 1500 Å thick undoped layer and again a heavily doped 1000 Å-wide in-situ doped layer (Fig. 3). The heavily doped grain boundaries ($N \sim 10^{20}$ cm^{-3}) within the lightly doped grains create a high-low junction with low effective recombination velocity [25], thus only slightly affecting the current flow.

If the minority holes were to diffuse across the about 200-300 Å thick interfacial layer into the low-doped region, the expected current from (8) would be much larger than for the in-situ doped devices, because N_e(poly) << 10^{18} cm^{-3} in the low-doped grains. The measured hole currents for the in-situ doped and bilayer devices are, however, almost equal. The exceptions are the bilayer devices where the heat treatment was not sufficient to obtain high arsenic concentration at the interface. The differences in the values of J_{po} of less than about a factor of two between the bilayer devices 1J, 1L and the in-situ doped devices, can be attributed to small variations in W_{epi}, τ_p(epi), and mainly N_{DD}. The average doping density in the epitaxial layers was measured by the C-V technique and varied from about 9×10^{15} cm^{-3} to about 2×10^{16} cm^{-3}. This fact is also reflected in the spread of the J_{po} values for the devices with the metal contact which was in the range from about 4×10^{-10} A/cm^2 to about 6×10^{-10} A/cm^2.

The preliminary conclusions (1) and (2) in Section IV-A and the discussion in this section lead to the following:

(i) The minority carrier transport at the polysilicon-monosilicon interface with no intentional insulating layer at the interface is determined by the carrier transport within the polysilicon, rather than by a tunneling through an insulating layer.

(ii) The similarity of the electrical properties of the devices with the in-situ doped and the bilayer polysilicon films suggests a correlation between the electrical properties and the microstructure of the very thin interfacial layer within about 200 - 300 Å of the metallurgical interface in the polysilicon film. It also suggests that most of the minority carriers crossing the $x = W_{epi}$ plane (Fig. 4) recombine within 200 - 300 Å of the metallurgical interface.

(iii) In order to explain J_p(polysilicon contact) << J_p(n^+ monosilicon), the heavily-doped interfacial layer must have properties significantly different from the properties of the monosilicon.

(iv) The dominant mechanism responsible for low J_p(polysilicon contact) is much more sensitive to the arsenic dopant concentration at the interface than to the carrier electron concentration at the interface.

The polysilicon-monosilicon interface can be regarded as a region with a high degree of disorder. This is due largely to the very sudden transition from the orderly epitaxial single crystal layer to the CVD-deposited polysilicon with the randomly oriented (without prefered orientation) grains of a few hundred Angstroms in size. It was recently observed by means of cross-sectional TEM that the arsenic doped polysilicon-monosilicon interface

consists in some cases of a crystalline phase with about 40 Å average grain size, compared to ~ 400 Å in the bulk of the polysilicon film, while in some other cases this interface is amorphous [22,26]. It is well known that the disordered regions of semiconductors are associated with low carrier mobilities (and diffusivities). As an example, the drift majority-carrier mobilities in amorphous Si are $\mu_n \simeq (2\text{-}5) \times 10^{-2}$ cm^2/Vs and $\mu_p \simeq 5 \times 10^{-4}$ cm^2/VS [27]. Even smaller values are expected for minority carriers.

The disorder contributes to the random component in the atomic potential which results in band tails [28]. Trapping by band tails was identified as one of the possible mechanisms causing very low mobility in amorphous Si [27]. Band tails can be responsible for low minority-carrier mobility by a process of trapping also in heavily doped single crystal Si, as was recently suggested [29].

The microstructure at the interface and the electrical measurements lead us to a proposal for a possible mechanism of current suppression by the polysilicon contact: very low minority carrier mobility (and diffusivity) in the very highly doped and disordered interfacial region. Note that both amorphous structure and very small grains at the interface predict low mobility.

Because of the large sensitivity of our test structure to the interface, we can make a better estimate of the minority-carrier mobility in the polysilicon than made before in [3]. In order to do that we have to have a reasonable model for the recombination current $Q_p(int)/\tau_p(int)$ in the interfacial layer. We assume again that, as a first approximation, this current can be described as a diffusion current

$$\frac{Q_p(int)}{\tau_p(int)} \simeq \frac{qn_i^2}{N_e(int)} \frac{D_p(int)}{\tau_p(int)} \lesssim 10^{-13} \text{ A/cm}^2 \quad . \tag{9}$$

The quantity on the right-hand side of (9) results from (7). Approximating the parameters in (9) by a single crystal Si values, we have $N_e \sim 10^{18}\ cm^{-3}$ [18], and $\tau_p(int) \sim \tau_A \simeq 2 \times 10^{-10}$ sec [30], where τ_A is the Auger lifetime. Equation (9) then implies the upper limits for

$$D_p(int) \sim 5 \times 10^{-3}\ cm^2/s \qquad (10a)$$

and

$$L_p(int) \sim 100\ \text{Å} \quad . \qquad (10b)$$

Thus, $D_p(int)$ from (9) and (10a) is about 3 orders of magnitude smaller than the single crystal value.

The rough approximations of (10a), (10b) do not take into account the consequences of the detailed microstructure of the interface, but they do, nevertheless, lend support to the interpretation based on the possibility of large gradient in the minority-carrier diffusivity at the polysilicon-monosilicon interface. This mechanism will greatly suppress the current. The minority carriers will then recombine very close to the metallurgical polysilicon-monosilicon junction without the possibility to diffuse deep into the polysilicon.

An alternative explanation can be offered by an interface in a heterojunction form with a very large barrier for holes. The heterojunction can be created because of a position-dependent chemical composition giving rise to spatial variations of the bandgap, electron affinity and the band edges of the conduction and valence bands [31]. As an example, if a thin

(~ 20 Å) amorphous layer exists at the interface [22,26], a discontinuity of the bandgap and electron affinity may result. To further analyse such a structure would, however, require much more detailed information about the chemical and electronic structure of the interface than presently available.

Even though the heterojunction model or the tunneling model [2] cannot be excluded as a possibility, there are however two findings that point particularly in the direction of the low mobility model. First, the finding of the correlation between the recombination current and the dopant arsenic density agrees with studies which show that at the microscopic level the atomic potential has a random component because of the random distribution of impurities whether impurities are ionized or not [32]. Second, the observation by Ning and Isaac [3] of the dependence of the base current in the bipolar transistor on the polysilicon thickness. A noticeable increase in the base current was observed for transistors with the polysilicon film thickness of 300 Å or less. This observation agrees with our model of carrier recombination within the interfacial region, such as illustrated in Fig. 3 for the bilayer film structure.

The undoped polysilicon contacts in devices 1E - 1G behave as interfaces with very large recombination velocity with current densities about equal to the current densities for the reference metal contacts (see Table I). This is expected because the potential profile at the interface between the epitaxial layer with $N \simeq N_{DD} \simeq 10^{16}$ cm^{-3} and the polysilicon with $N < 10^{16}$ cm^{-3} creates an electric field in the direction of the hole flow, thus aiding holes across the interface. The recombination current inside of the undoped contacts is expected to be large because of low electron density and small grain size (~ 100 Å), as (9) implies. The above arguments apply also to the bilayer devices 1I and 1K.

It is very convenient to characterize the polysilicon-monosilicon interface by the effective surface recombination velocity S_p at the high-low junction in the epitaxial layer at $x = W_{epi}$ (Fig. 4), which is defined as [33]

$$S_p = J_p(W_{epi})/q\Delta P(W_{epi}) \tag{11}$$

where $\Delta P(W_{epi})$ is the excess hole density and $J_p(W_{epi})$ is the current density at $x = W_{epi}$. The value of S_p cannot be deduced exactly without a precise knowledge of $\tau_p(epi)$, since the bulk recombination in the epitaxial layer is not negligible in our devices, but is in fact dominant. An approximate value of $S_p \sim 15$ cm/sec was deduced before. For many purposes, however, an upper limit of S_p is sufficient. This upper limit can be obtained exactly from (6) by neglecting the bulk losses (i.e. by setting $W_{epi}/\tau_p(epi) = 0$), or from

$$S_{pmax} = \frac{D_p/W_{epi}}{(J_p(\Omega)/J_p)} \tag{12}$$

where $J_p(\Omega) = [(qn_i^2 D_p)/(N_{DD}W_{epi})] \exp(qV/kT)$ is the current for the reference device with the metal contact. The upper limit values for S_p calculated from (12) are listed in Table I.

From the upper limit of S_p given by (12) we can also estimate the upper limit of the effective surface recombination velocity at the n^+ polysilicon-n^+ monosilicon metallurgical interface. Assuming that the thin n^+ outdiffused monosilicon layer is essentially transparent we obtain from $J_p(W_{epi}) \simeq J_p(n^+ \text{ poly-}n^+)$

$$S_p(n^+\text{poly-}n^+) \simeq S_p \frac{N_e(int)}{N_{DD}(epi)} \simeq \sqrt{\frac{D_p(int)}{\tau_p(int)}} < 10^4 \text{ cm/sec} \tag{13}$$

where $N_e(int)/N_{DD}(epi) \simeq 10^{18}\ cm^{-3}/10^{16}\ cm^{-3} \simeq 100$ [18]. Using the approximate value of $S_p \sim 15$ cm/sec in (13) yields $S_p(n^+poly\text{-}n^+) \simeq$ 1500 cm/sec.

The n^+ polysilicon contact on the top of the n^+ diffused or implanted monosilicon emitter in the bipolar transistor can be also characterized by (13), since (13) reflects the recombination in the polysilicon independently of the doping in the monosilicon. The low value for $S_p(n^+poly\text{-}n^+)$ in comparison with $S_p \sim 10^6$ cm/sec for the ohmic metal contact explains, qualitatively, the improved current gain in bipolar transistors with polysilicon contacts to thin emitters.

IV. SUMMARY

In this work, we have presented the results of a detailed experimental study of a polysilicon-monosilicon contact. The purpose of this study was to explain both qualitatively and quantitatively the mechanism of improved current gain in bipolar transistors with polysilicon contacts. The study correlates the microstructure of the polysilicon-monosilicon junction with the electrical properties. The electrical properties were measured using p/n junction test structures (Fig. 1) that are much more sensitive to the contact properties than are bipolar transistors.

Correlation of the electrical results with the microstructure yielded the conclusion that the minority-carrier transport in the polysilicon-monosilicon junction is controlled by a highly disordered layer within $\sim$ 100 Å of the interface characterized by very low minority-carrier diffusivity. This conclusion confirms the model of Ning and Isaac that explained the improved current gain by $D_p(n^+$ polysilicon$)/ D_p(n^+$ monosilicon$) \simeq 0.3$. The present results indicate, however, that the effective D_p in the n^+ polysilicon has to

be substantially smaller than the corresponding value in the n^+ monosilicon to obtain the quantitative agreement with the data: $D_p(n^+$ polysilicon$)/D_p(n^+$ monosilicon$) \sim 5 \times 10^{-3}$. The effective surface recombination velocity for minority holes at the n^+ polysilicon-n^+monosilicon interface was found to be much smaller ($\lesssim 10^4$ cm/s) than the kinetic limit value for ohmic contact ($\sim 5 \times 10^6$ cm/sec).

We did not study the effects of surface treatments prior to polysilicon deposition, namely the effects of thin interfacial oxide layer [2,7].

The saturation current density in the polysilicon contact was found to be less than about 10^{-13} A/cm^2 at 25°C. The typical value of the saturation collector current density in the bipolar transistor with basewidth of about 0.1 μm, base sheet resistance of about 8 kΩ/square and current gain $\beta \approx 100$ is about 10^{-10} A/cm^2 [3]. This implies that current gains $\beta > 1000$ are possible, provided that the recombination losses in the n^+ monosilicon emitter can be suppressed, for example by reducing the width of the n^+ monosilicon region [2,34].

The sensitivity of the test structures used in this study to the polysilicon contact and the accuracy of the method used to separate the current components was limited mainly by the minority-carrier lifetime in the epitaxial layer. More conclusive experiments [21] using devices with varying widths and dopings of the epitaxial layer would be desirable to improve the accuracy of the analysis.

A very low effective surface recombination velocity for the minority carriers at the polysilicon-monosilicon interface suggests applications of polysilicon contacts in devices other than bipolar transistors. An example could be a back-surface-field solar cell in which the recombination losses at the back high-low monosilicon contact can limit the cell efficiency.

ACKNOWLEDGMENTS

The authors wish to express their appreciation to B. Ginsberg, R. Shultz, M. Smyth and all other members of the silicon facility for their technical assistance. We also wish to thank T. H. Ning, D. D. Tang, and H. Stork for helpful discussions.

One of the authors (A.N.) would like to thank Professor F. A. Lindholm for many valuable discussions related to this work. One of the authors (A.N.) also wishes to acknowledge the support of the National Science Foundation under Grant No. ECS-8203091 and the support of the Jet Propulsion Laboratory under Contract No. 956525.

REFERENCES

1. J. Graul, A. Glasl, and M. Murmann, "High performance transistors with arsenic-implanted polysil emitters", IEEE J. Solid-State Circuits, vol. SC-11, p. 491, Aug. 1976.

2. H. C. de Graaff and J. G. de Groot, "The SIS tunnel emitter: A theory for emitters with thin interface layers", IEEE Trans. Electron Devices, vol. ED-26, p. 1771, Nov. 1979.

3. T. H. Ning and R. D. Isaac, "Effect of emitter contact on current gain of silicon bipolar devices", IEEE Trans. Electron Devices, vol. ED-27, p. 2051, Nov. 1980.

4. J. G. Fossum and M. A. Shibib,"A minority carrier transport model for polysilicon contacts to silicon bipolar devices, including solar cell", in IEDM Tech. Dig., p. 280, 1980.

5. A. A. Eltoukhy and D. J. Roulston, "The role of the interfacial layer in polysilicon emitter bipolar transistors", IEEE Trans. Electron Devices, vol. ED-29, pp. 1862-1869, Dec. 1982.

6. P. H. Yeung and W. C. Ko, "Current gain in polysilicon emitter transistors", IEEE Trans. Electron Devices, vol. ED-30, pp. 593-597, June 1983.

7. B. Soerowirdjo and P. Ashburn, "Effects of surface treatments on the electrical characteristics of bipolar transistors with polysilicon emitters", Solid-State Electron., vol. 26, pp. 495-498, May 1983.

8. Z. Yu, B. Ricco', and R. W. Dutton, "A comprehensive analytical and numerical model of polysilicon emitter contacts in bipolar transistors", IEEE Trans. Electron Devices, vol. ED-31, pp. 773-784, June 1984.

9. M. Arienzo, Y. Komem, and A. E. Michel, "Diffusion of arsenic in bilayer polycrystalline silicon films", J. Appl. Phys., vol. 55, pp. 365-369, Jan. 1984.

10. C. R. M. Grovener, P. E. Batson, D. A. Smith, and C. Y. Wong, to be published in Philosophical Magazine.

11. T. W. Hickmott and R. D. Isaac, "Barrier height at the polycrystalline silicon-SiO_2 interface", J. Appl. Phys., vol. 52, pp. 3464-3475, May 1981.

12. J. Murota and T. Sawai, "Electrical characteristics of heavily arsenic and phosphorous doped polycrystalline silicon", J. Appl. Phys., vol. 53, pp. 3702-3708, May 1982.

13. A. Neugroschel, F. A. Lindholm, C. T. Sah, "A method for determining the emitter and base lifetimes in p-n junction diodes," IEEE Trans. Electron Devices, vol. ED-24, pp. 662-671, June 1977.

14. W. Rosenzweig, "Diffusion length measurement by means of ionizing radiation", Bell Syst. Techn. J., vol. 41, pp. 1573-1588, Sept. 1962.

15. J. Y. W. Seto, "Electrical properties of polycrystalline silicon films", J. Appl. Phys., vol. 46, pp. 5247-5254, Dec. 1975.

16. G. Baccarani and B. Ricco, "Transport properties of polycrystalline silicon films", J. Appl. Phys., vol. 49, pp. 5565-5570, Nov. 1978.

17. H. C. Card, E. S. Yang, "Electronic processes at grain boundaries in polycrystalline semiconductors under optical illumination", IEEE Trans. Electron Devices, ED-24, pp. 397-402, April 1977.

18. A. Neugroschel, S. C. Pao, and F. A. Lindholm, "A method for determining energy gap narrowing in highly doped semiconductors", IEEE Trans. Electron Devices, vol. ED-29, pp. 894-902, May 1982.

19. M. A. Shibib, F. A. Lindholm, and F. Therez, "Heavily doped transparent-emitter regions in junction solar cells, diodes, and transistors", IEEE Trans. on Electron Devices, vol. ED-26, pp. 959-965, June 1979.

20. N. D. Arora, J. R. Hauser, and D. J. Roulston, "Electron and hole mobilities in silicon as a function of concentration and temperature", IEEE Trans. Electron Devices, vol. ED-29, pp. 292-295, Feb. 1982.

21. F. N. Gonzalez and A. Neugroschel, "Measurement of diffusion length, lifetime and surface recombination velocity in thin semiconductor layers", accepted for publication in IEEE Trans. Electron Devices, April 1984.

22. C. Y. Wong, A. E. Michel, and R. D. Isaac, "The poly-single crystalline silicon interface", J. Appl. Phys., vol. 55, pp. 1131-1134, Feb. 1984.

23. F. A. Lindholm and J. G. Fossum, "Pictorial derivation of the influence of degeneracy and disorder on nondegenerate minority-carrier concentrations and recombination current in heavily doped silicon", IEEE Electron Device Lett., vol. EDL-2, pp. 230-234, Sept. 1981.

24. D. D. Tang and A. Mickel, "Effects of impurity compensation on injection current in Si bipolar transistors", IEEE Trans. Electron Devices, vol. ED-27, pp. 1836-1838, Sept. 1980.

25. A. Neugroschel and J. A. Mazer, "Effects of grain boundaries on the current-voltage characteristics of polycrystalline silicon solar cells", IEEE Trans. Electron Devices, vol. ED-29, pp. 225-236, Feb. 1982.

26. C. Y. Wong and Y. Komem, unpublished work.

27. Amorphous Semiconductors, edited by M. H. Brodsky, Springer-Verlag, New York, 1979, Chapters 9, 10.

28. E. O. Kane, "Thomas-Fermi approach to impure semiconductor band structure," Phys. Rev., vol. 131, pp. 79-88, 1963.

29. A. Neugroschel and F. A. Lindholm, "Evidence for low diffusivity and mobility of minority carriers in highly doped Si and interpretation", Appl. Phys. Lett., vol. 42, pp. 176-178, Jan. 1983.

30. J. Dziewior and W. Schmid, "Auger coefficients for highly doped and highly excited silicon", Appl. Phys. Lett., vol. 31, pp. 346-348, Sept. 1, 1977.

31. C. T. Sah and F. A. Lindholm, "Carrier generation, recombination, trapping, and transport in semiconductors with position dependent composition", IEEE Trans. on Electron Devices, vol. ED-24, pp. 358-362, April 1977.

32. H. Fritzche, "The metal-non-metal transitions in disordered systems", in the Proceedings of the 19th Scottish Summer School in Physics, edited by L. R. Friedman and D. P. Tunstall, August 1978.

33. See for example J. R. Hauser and P. M . Dunbar, "Minority carrier reflecting properties of semiconductor high-low junctions", Solid-State Electronics, vol. 18, pp. 715-716, July 1975.

34. M. A. Green and R. B. Godfrey, "Super-gain silicon heterojunction emitter transistors", IEEE Electron Device Lett., vol. EDL-4, pp. 225-227, July 1983.

TABLE I

Summary of heat treatments and electrical measurements. Heat treatments for poly-silicon contacts were performed in argon. Electrical measurements were done at 25°C.

CONTACT	DEVICE	HEAT TREATMENT	J_{po} (10^{-13}A/cm^2)	S_{pmax} (cm/sec)
Undoped	1E	none	$(5.8 \pm 0.4) \times 10^3$	$\sim 10^6$
Polysilicon	1F	800°C, 64 hrs	$(5.5 \pm 0.5) \times 10^3$	$\sim 10^6$
(1500 A)	1G	900°C, 5 min	$(5.5 \pm 0.5) \times 10^3$	$\sim 10^6$
In-situ	1A	none	7 ± 0.3	175
Doped	1B	800°C, 64 hrs	10 ± 1.5	250
Polysilicon	1C	900°C, 5 min	6.6 ± 0.5	175
(1500 A)	1D	900°C, 15 min	6.5 ± 0.3	165
	2BE	1000°C, 15 min	6 ± 0.5	165
Bilayer:	1I	none	$(4.2 \pm 0.2) \times 10^3$	$\sim 10^6$
1500 Å undoped +	1J	800°C, 64 hrs	4.9 ± 0.6	175
1000 Å in-situ	1K	900°C, 15 min	$(4.2 \pm 0.2) \times 10^3$	$\sim 10^6$
doped	1L	850°C, 14 hrs	5.2 ± 0.6	180
	2BA	750°C, 8 hrs	$(4.0 \pm 0.3) \times 10^3$	$\sim 10^6$
Metal Reference		450°C, 20 min	$(5 \pm 1) \times 10^3$	$\sim 10^6$

FIGURE CAPTIONS

Fig. 1 Cross-sectional view of devices used in this study.

(a) Device with polysilicon contact film;

(b) Reference device with metal contact only. The broken lines in (a), (b) show the implanted n^+-contact ring in the epitaxial layer. Devices with and without the contact rings were fabricated on the same wafer.

Fig. 2 SIMS profiles of the arsenic distributions [8] for:

(a) The in-situ doped polysilicon with no heat treatment;

(b) The bilayer film before heat treatment (1I) and after 750°C, 8 hrs (2BA) and 850°C, 64 hrs (1J) heat treatments. The extent of the As profile into the monosilicon is not larger than the resolution of the SIMS equipment which is about 1 decade per 100 Å [9].

Fig. 3 Schematic illustration of the arsenic concentration profile in the vicinity of the polysilicon-monosilicon metallurgical interface for the bilayer film after heat treatment. The shaded areas show the preferentially doped regions around the grain boundaries and the arsenic diffusion into the monosilicon. The broken lines depict the width of the arsenic diffusion from the grain boundary monolayer to the bulk of the grains. The screened area within the interfacial layer symbolizes the fact that the microstructure of the polysilicon film in this area is very different from the microstructure in the rest of the polysilicon film.

Fig. 4 (a) Schematic illustration of a forward biased test structure with heavily-doped n^+polysilicon contact showing the separation of the polysilicon film into two layers: the interfacial layer and the polysilicon bulk.

(b) Band diagram for the forward bias.

(c) Profile of the minority hole concentration for the case of low effective recombination velocity at $x = W_{epi}$. The broken line depicts the approximate decay of the minority holes in the polysilicon.

Fig. 5 Current-voltage dependencies for several devices with polysilicon contact and for the reference device with metal contact.

Fig. 6 Current-voltage characteristics for devices with bilayer polysilicon contact.

Fig. 7 Activation plots [18] of $C(I_{po}/T^m)[\exp(\eta_c)/F_{1/2}(\eta_c)] = \exp[-(E_{GI}/(0) - \Delta E_G)/kT] = \exp(-E_G/kT)$ versus 1000/T for devices with undoped, in-situ doped, and bilayer polysilicon contacts. Activation plots for the device with reference metal contact and for the reference n^+/p monosilicon junction are also shown. The slopes yield $E_G \approx 1.206 \pm 0.03$ eV for the metal reference device and for the polysilicon devices 1B, 1J, and 1F. The slope for the n^+/p monosilicon device yields $E_G \approx 1.071 \pm 0.025$ eV.

Fig. 8 The dependence of $S_p + W_{epi}/\tau_p(epi)$ on the thickness of the epitaxial layer W_{epi}. The extrapolation to $W_{epi} \to 0$ yields $S_p \sim 15$ cm/sec.

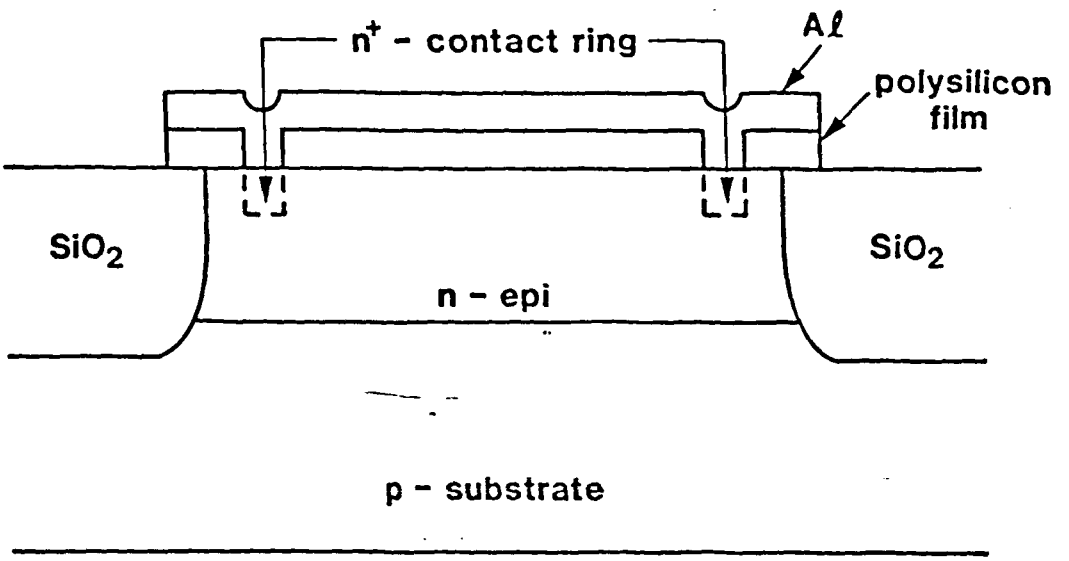

(a)

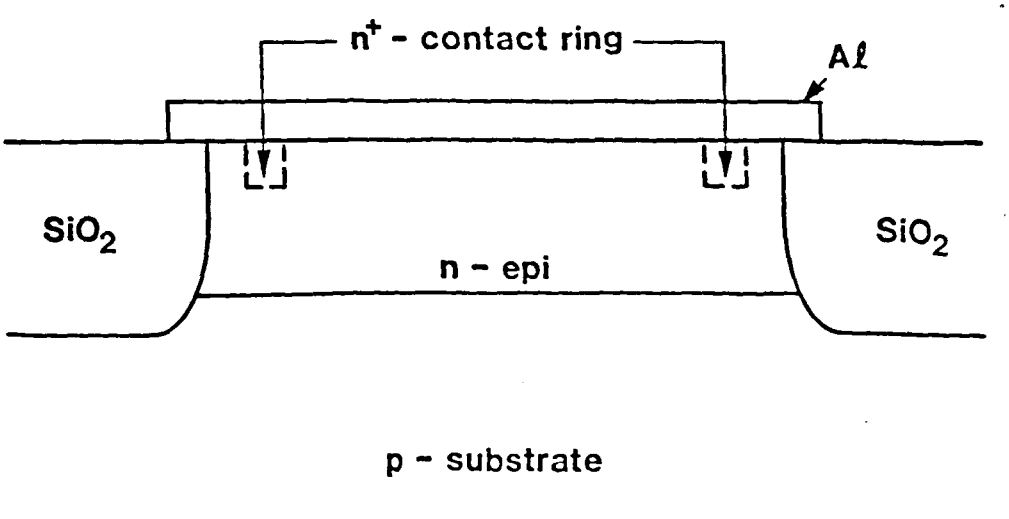

(b)

FIG. 1

Neugroschel et. al.

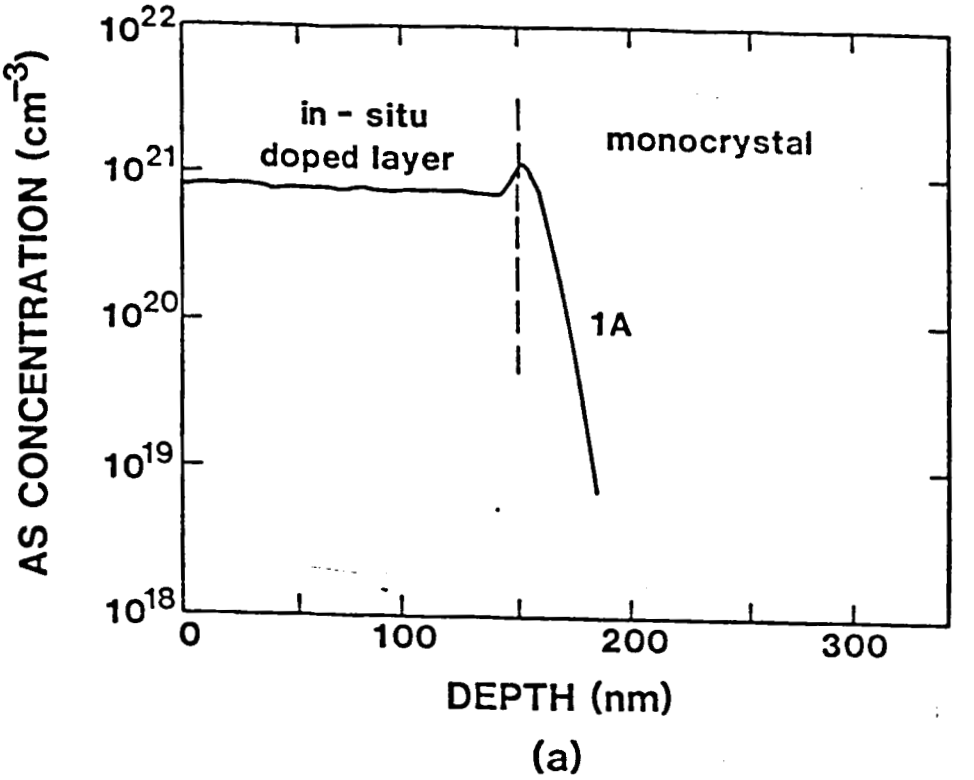
AS CONCENTRATION (cm^{-3})
10^{22}
10^{21}
10^{20}
10^{19}
10^{18}
in - situ
doped layer
monocrystal
1A
0
100
200
300
DEPTH (nm)

(a)

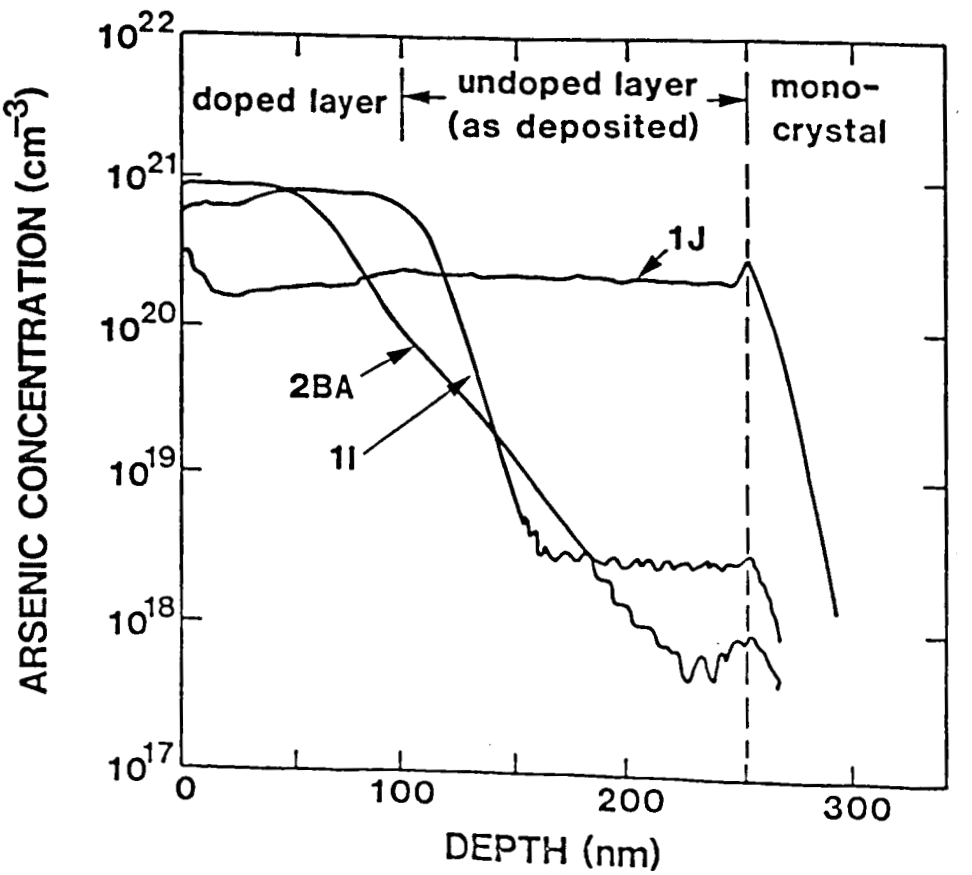
ARSENIC CONCENTRATION (cm^{-3})
10^{22}
10^{21}
10^{20}
10^{19}
10^{18}
10^{17}
doped layer
undoped layer
(as deposited)
mono-
crystal
1J
2BA
1I
0
100
200
300
DEPTH (nm)

(b)

FIG 2

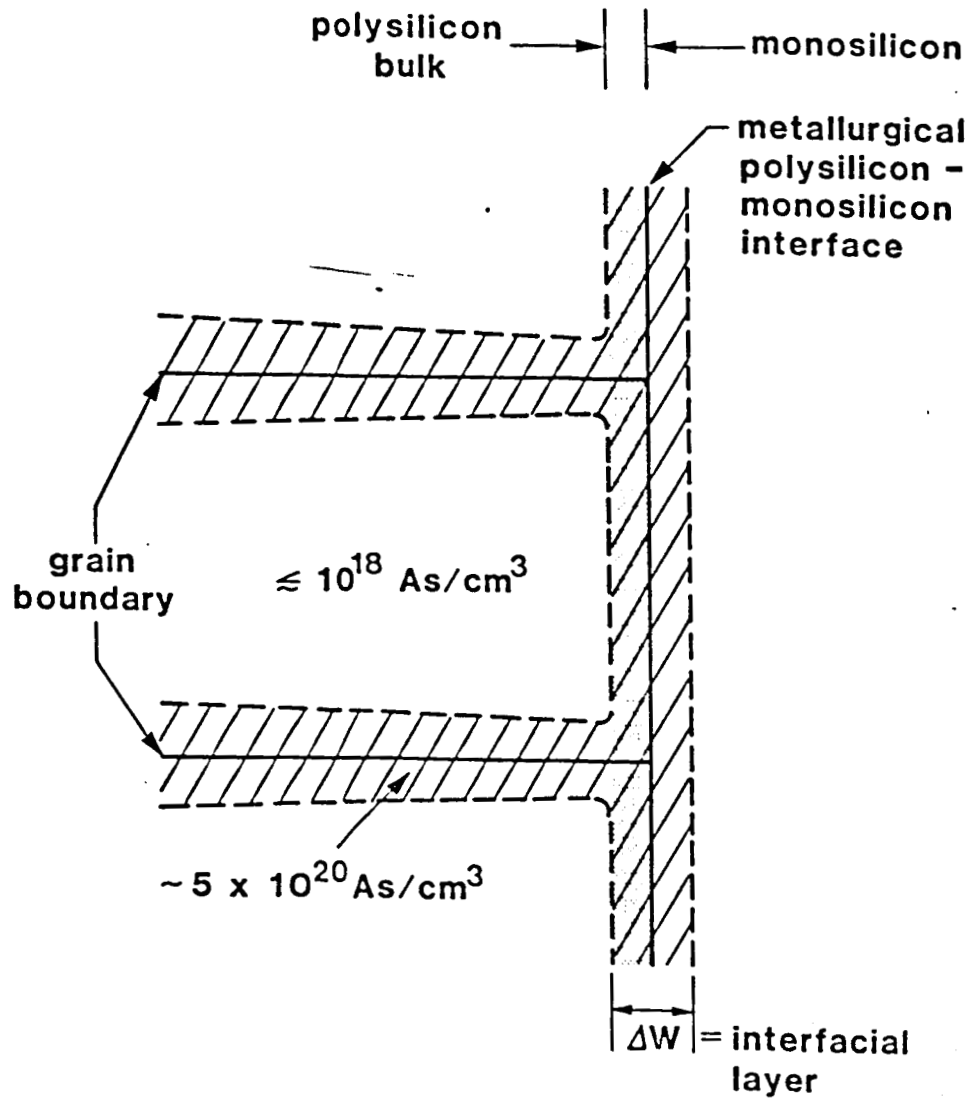
polysilicon bulk
monosilicon
metallurgical polysilicon - monosilicon interface
grain boundary
≲ 10^18 As/cm^3
~5 x 10^20 As/cm^3
ΔW = interfacial layer

FIG. 3

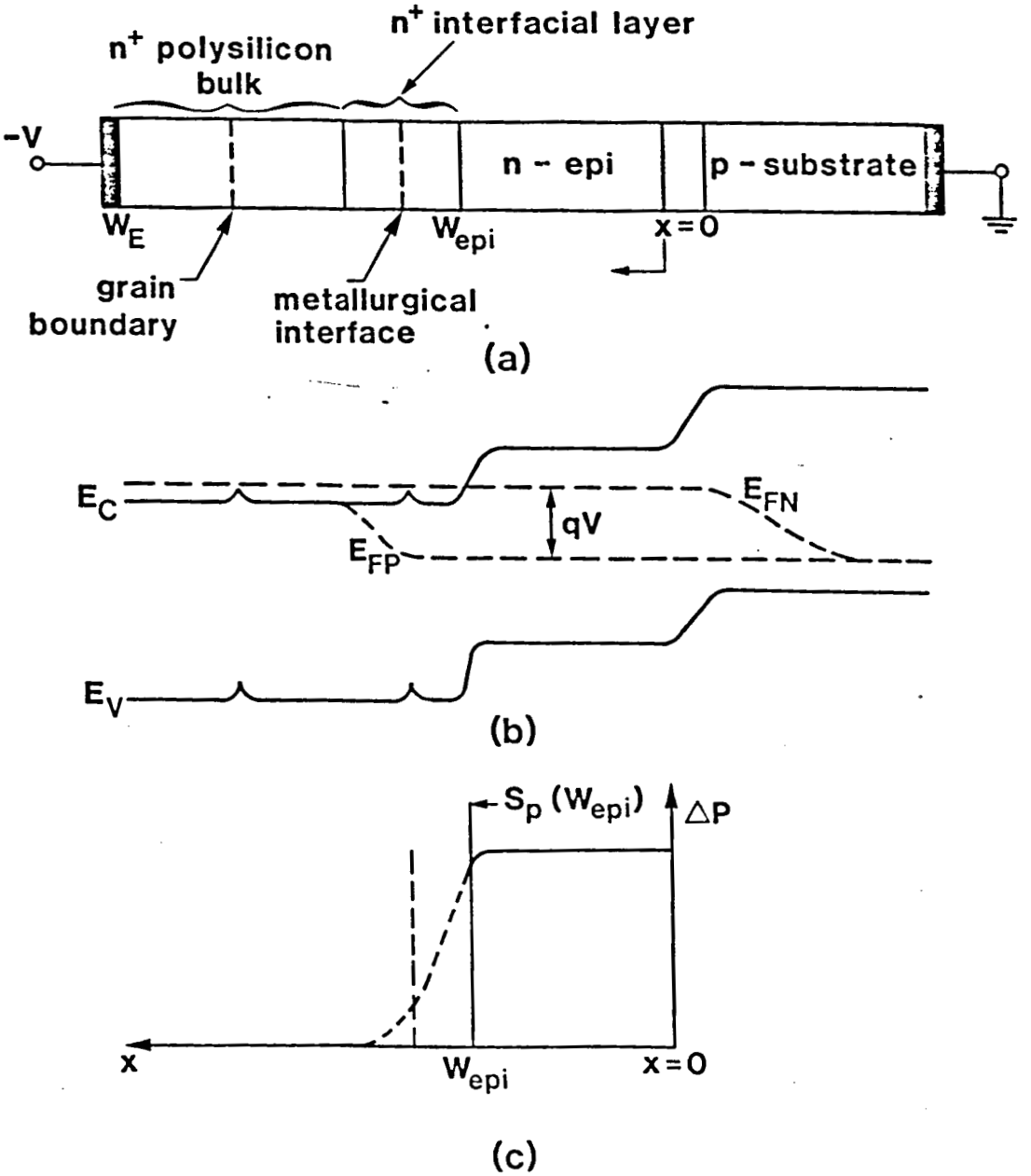
n+ interfacial layer
n+ polysilicon bulk
-V
n - epi
p - substrate
W_E
W_epi
x=0
grain boundary
metallurgical interface
(a)
E_C
E_FN
qV
E_FP
E_V
(b)
S_p (W_epi)
ΔP
x
W_epi
x=0
(c)

FIG. 4

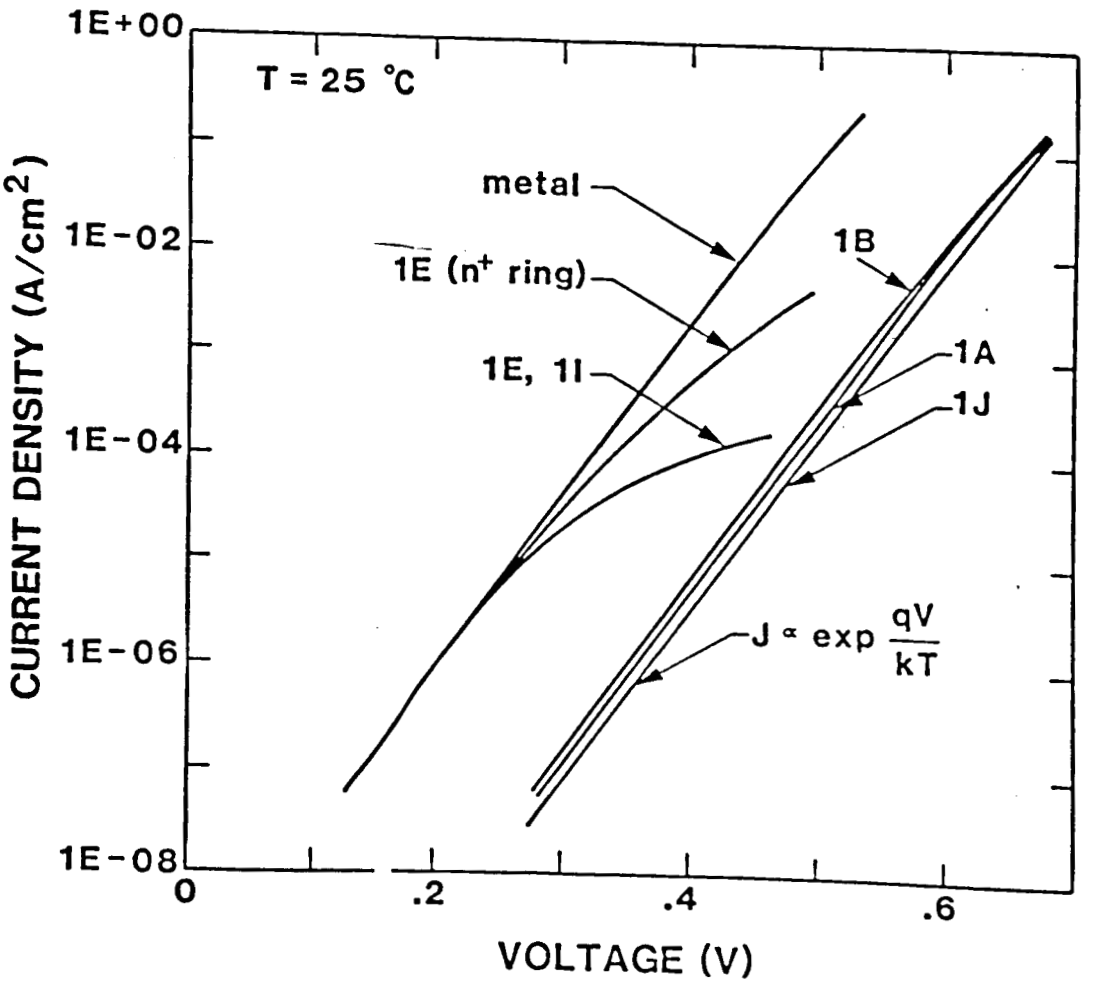
1E+00
1E-02
1E-04
1E-06
1E-08
CURRENT DENSITY (A/cm²)
T = 25 °C
metal
1E (n⁺ ring)
1E, 1I
1B
1A
1J
J ∝ exp qV/kT
0
.2
.4
.6
VOLTAGE (V)

FIG. 5

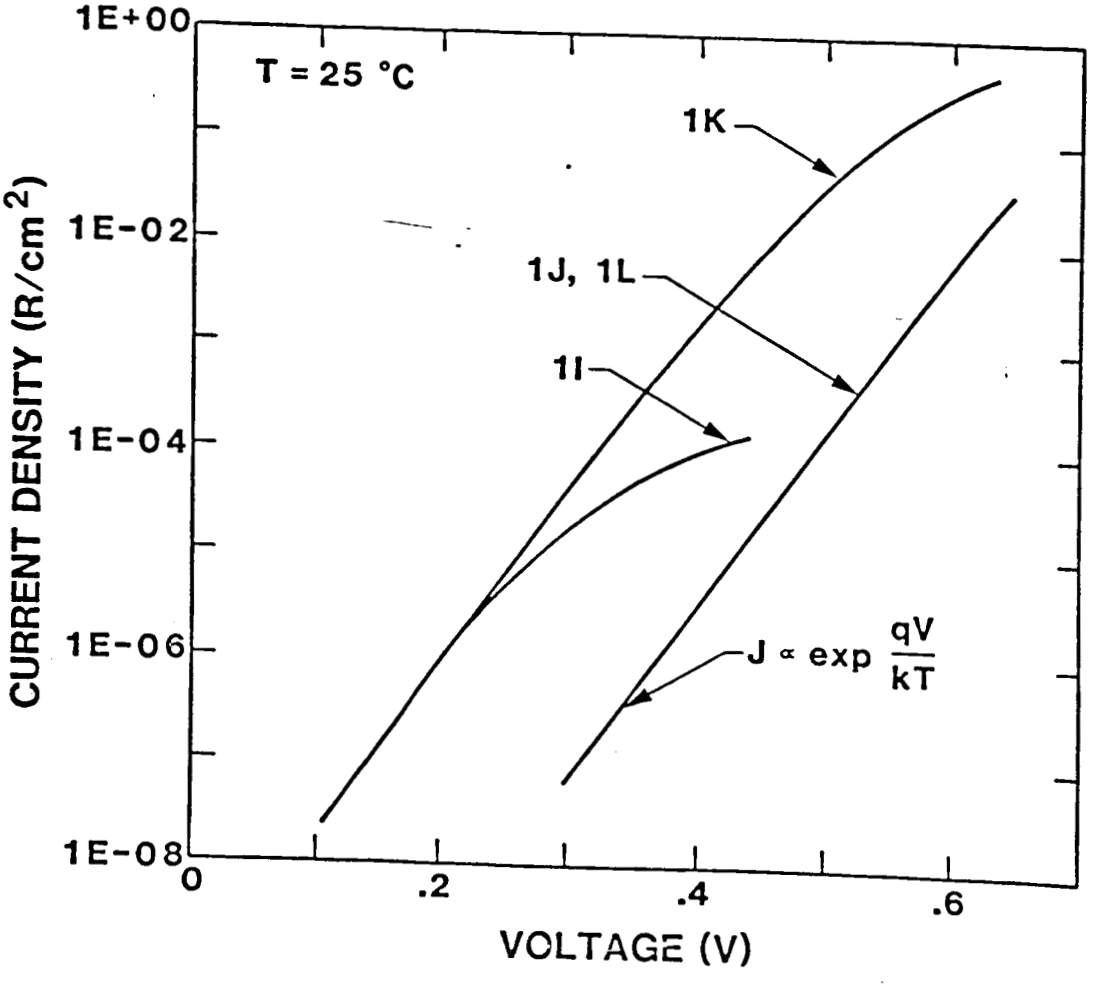
1E+00
1E-02
1E-04
1E-06
1E-08
CURRENT DENSITY (R/cm²)
T = 25 °C
1K
1J, 1L
1I
J ∝ exp qV/kT
0
.2
.4
.6
VOLTAGE (V)

FIG. 6

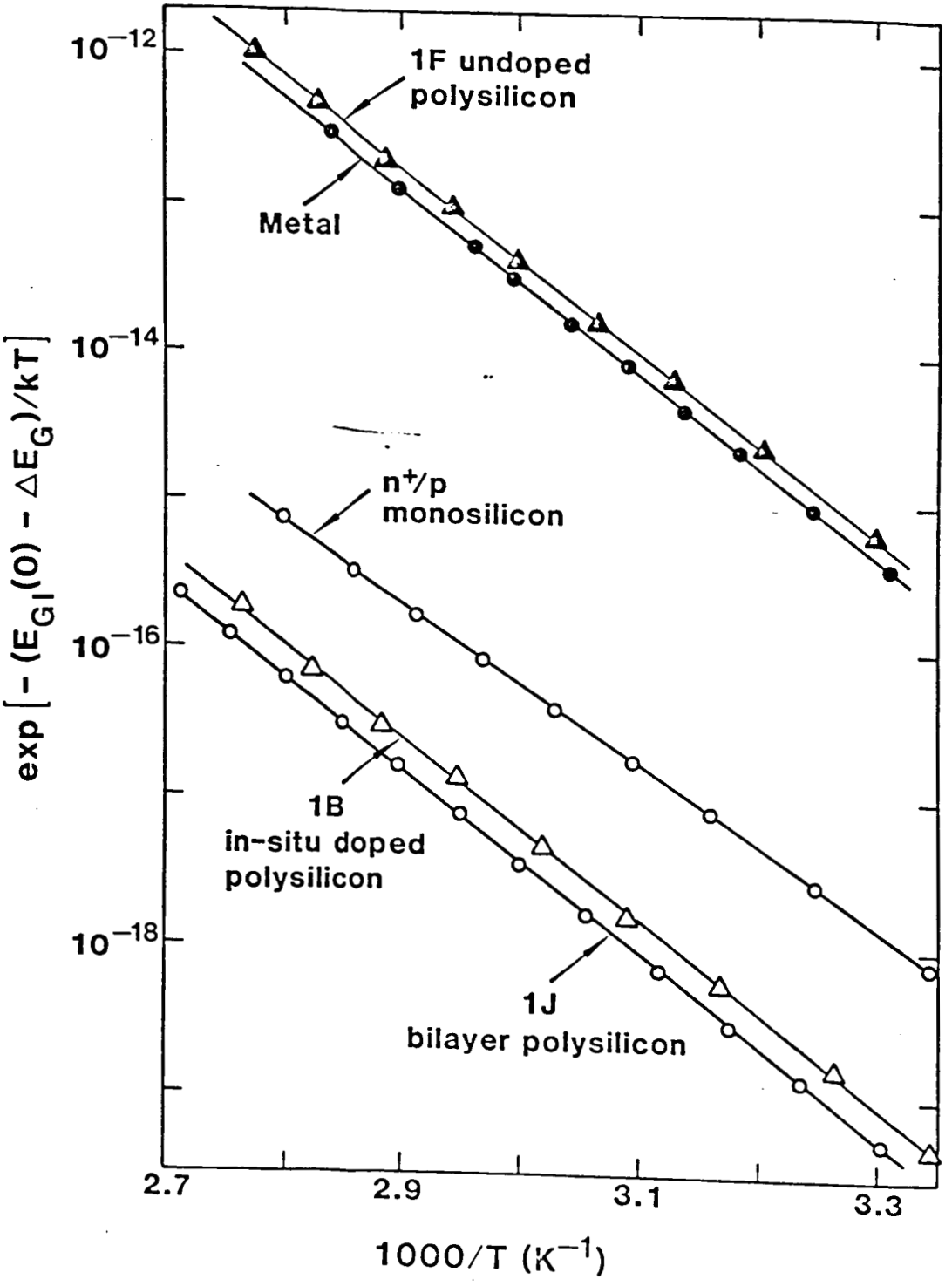
10^{-12}
10^{-14}
10^{-16}
10^{-18}
$\exp\left[-(E_{GI}(0) - \Delta E_G)/kT\right]$
1F undoped polysilicon
Metal
n^+/p monosilicon
1B in-situ doped polysilicon
1J bilayer polysilicon
2.7
2.9
3.1
3.3
1000/T (K^{-1})

FIG. 7

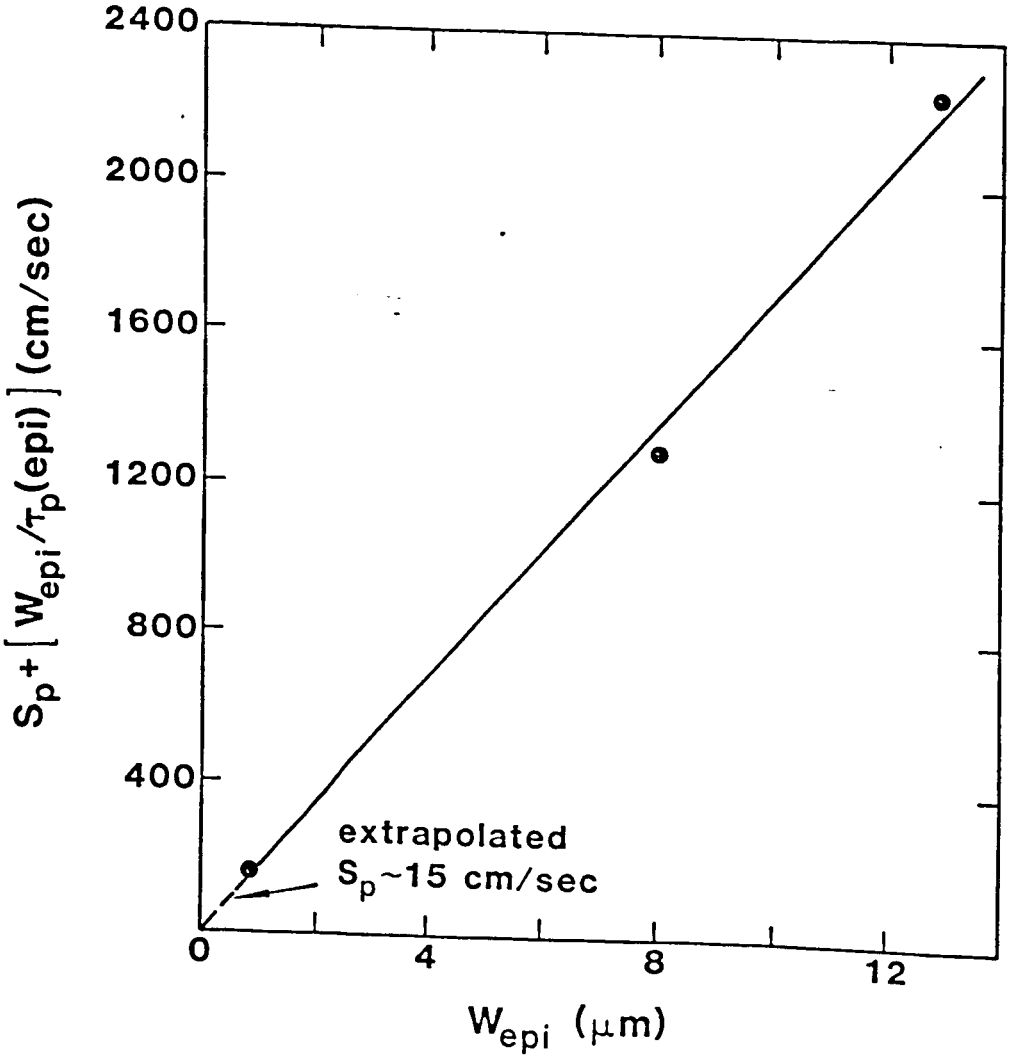
2400
2000
1600
1200
800
400
0
4
8
12
$S_p + [W_{epi}/\tau_p(epi)]$ (cm/sec)
W_{epi} (μm)
extrapolated
S_p~15 cm/sec

FIG. 8

CHAPTER FOUR
SOLUTION OF THE CONTINUITY EQUATION IN PLANAR SYMMETRY CASES AND ASSESSMENT OF PHOTOLUMINESCENCE DECAY

I. INTRODUCTION

Photoluminescence decay is one of the methods used in determining the minority carrier lifetime in heavily doped silicon [1]. The method consists of exciting a silicon sample by a laser pulse and thus generating excess electron-hole pairs. The lifetime is derived from the decay rate of the excess charge. This decay as a function of time is obtained by monitoring the radiation emitted by the few electron-hole pairs that recombine through radiative recombination. In principle, this method is more reliable than many other methods because it involves no assumptions regarding the band structure and the transport parameters in heavily doped silicon. On the other hand, the method has the drawback that surface recombination prohibits the decay from being purely expoential. Moreover, the effect on the decay rate of the size and shape of the laser beam was not clarified previously.

Recent papers [2,3] have investigated the time dependence of the luminescence decay, and in particular the influence of surface recombination on the decay rate for special types of excitation. In [2] the continuity equation is solved analytically for the total excess charge in the case of a finely focused beam, while in [3] the problem is simplified to one dimension by considering uniform excitation. In both cases it is found that the effect of the surface recombination can be minimized by waiting several lifetimes, after the laser is turned off, before measuring the decay rate.

In this work we extend the analysis of [2,3] for the general case of arbitrary excitation, and prove that the beam size, shape and uniformity does not affect the decay rate. An upper bound for the error due to surface recombination is derived. In agreement with [1,2,3] the effect of surface

recombination is found significant only in the initial part of the transient. In addition, as a preliminary result, a simplified form is given for the continuity equation when planar symmetry exists.

II. SOLUTION OF THE CONTINUITY EQUATION IN PLANAR SYMMETRY CASES

Figure 1 illustrates an infinitely extending semiconductor sample terminating at the z=0 and z=W planes. The laser beam shown is meant as an example of excitation. The following analysis is, in general, valid for any other type of excitation, for example, thermal generation, and minority-carrier injection over a potential barrier. The sample is n-type (extension to p-type is straightforward).

The continuity equation for holes is

$$\frac{\partial P}{\partial t}(x,y,z,t) = -\nabla\cdot\vec{J}_p(x,y,z,t) + G(x,y,z,t) - U(x,y,z,t) \qquad (1)$$

where $\vec{J}_p$ is the hole flux and G and U are generation and recombination rates in excess of their thermal equilibrium values. Integration of Eq. (1) over the $z = Z'(0 < Z' < W)$ plane yields

$$\frac{\partial Q}{\partial t}(Z',t) = -\int_{-\infty}^{\infty}\int_{-\infty}^{\infty} \nabla\cdot\vec{J}_p\,dxdy + \int_{-\infty}^{\infty}\int_{-\infty}^{\infty} G\,dxdy - \int_{-\infty}^{\infty}\int_{-\infty}^{\infty} U\,dxdy$$

$$= -\int_{-\infty}^{\infty}\int_{-\infty}^{\infty} \left(\frac{\partial j_{px}}{\partial x} + \frac{\partial j_{py}}{\partial y}\right)dxdy - \int_{-\infty}^{\infty}\int_{-\infty}^{\infty} \frac{\partial j_{pz}}{\partial z}\,dxdy +$$

$$+ \int_{-\infty}^{\infty}\int_{-\infty}^{\infty} G\,dxdy - \int_{-\infty}^{\infty}\int_{-\infty}^{\infty} U\,dxdy \quad . \qquad (2)$$

Here $Q(Z',t) = \int_{-\infty}^{\infty}\int_{-\infty}^{\infty} P(x,y,Z',t)dxdy$ is the number of holes per unit distance on the $z=Z'$ plane, and J_{px}, J_{py}, J_{pz} are the components of $\vec{J}_p = J_{px}\vec{x} + J_{py}\vec{y} + J_{pz}\vec{z}$. All of the integrals above are assumed to be finite.

By Gauss' theorem,

$$\int_{-\infty}^{\infty}\int_{-\infty}^{\infty}\left(\frac{\partial j_{px}}{\partial x} + \frac{\partial j_{py}}{\partial y}\right)dxdy = \int_{\Gamma_\infty}(j_{px}\vec{x} + j_{py}\vec{y})\cdot d\vec{s}$$

where Γ_∞ is the infinite circle on the $z=Z'$ plane, and $d\vec{s}$ is the infinitesimal vector normal to Γ_∞. The integral $\int_{\Gamma_\infty}(J_{px}\vec{x} + J_{py}\vec{y})\cdot d\vec{s}$ is the hole flux crossing the infinite circle, and is zero under restrictions on $G(x,y,z,t)$ that are nearly always obeyed. Therefore, Eq. (2) becomes:

$$\frac{\partial Q}{\partial t} = -\int\int \frac{\partial j_{pz}}{\partial z}dxdy + \int\int Gdxdy - \int\int Udxdy \qquad (3)$$

where from now on we omit the (infinite) limits of integration for brevity.

Expressing J_{pz} in terms of drift and diffusion and assuming that the electric field, diffusivity, and mobility (E_z, D_p, μ_p) are functions only of z and that the recombination rate is linear ($U = (P-P_0)/\tau$ with $\tau = \tau(z)$), we rewrite Eq. (3) as

$$\frac{\partial Q}{\partial t} = D_p\frac{\partial^2 Q}{\partial z^2} + \left[\frac{\partial D_p}{\partial z} - \mu_p E_z\right]\frac{\partial Q}{\partial z} - \left[\frac{\partial(\mu_p E_z)}{\partial z} + \frac{1}{\tau}\right]Q + \frac{Q_0}{\tau} + \int\int Gdxdy \quad . \quad (4)$$

Here $Q_0 = \int\int P_0 dxdy$ is the equilibrium number of holes per unit distance on the $z=Z'$ plane. If, in Eq. (4), P replaces Q and G replaces $\int\int Gdxdy$, the usual one-dimensional continuity equation results.

Equation (4) is a differential equation for the total charge on the z=Z' plane. It is linear provided E_z, D_p, μ_p are independent of the injection level (independent of P). Assuming this, we can rewrite Eq. (4) in terms of the number (per unit distance) of excess holes in the z=Z' plane, $Q' = \int\int \Delta P dxdy = Q - Q_0$:

$$\frac{\partial Q'}{\partial t} = D_p \frac{\partial^2 Q'}{\partial z^2} + \left[\frac{\partial D_p}{\partial z} - \mu_p E_z\right] \frac{\partial Q'}{\partial z} - \left[\frac{\partial (\mu_p E_z)}{\partial z} + \frac{1}{\tau}\right] Q' + \int\int G dxdy \quad . \quad (5)$$

Equation (5) results from Eq. (4) because $-D_p \, \partial P_0/\partial z + \mu_p \, E_z \, P_0 = 0$.

The recombination velocities S_1, S_2 of the front (z=0) and back (z=W) surface of the sample enter to determine the boundary conditions of Eq. (5):

$$S_1 \, Q'(t,0) = D_p \frac{\partial Q'}{\partial z}(t,0) \quad , \quad S_2 \, Q'(t, W) = -D_p \frac{\partial Q'(t,W)}{\partial z} \quad .$$

Under such boundary conditions the solution of Eq. (5) depends only on the total generation rate on the z=Z' plane ($\int\int G dxdy$) and not on G as a function of x and y. Knowledge of Q'(z,t) does not, of course, provide $\Delta P(x,y,z,t)$. However, it does provide the total minority current in the z direction, $I_z = -e \, D_p \, \partial Q'/\partial z + e \, \mu_p \, E_z \, Q'$, and the total number of excess holes,

$$\int\int\int \Delta P dv = \int_0^W Q' dz \quad .$$

Therefore, when one seeks to determine either the total minority current or the number of excess holes, Eq. (5) suffices, provided only that the transport parameters of the semiconductor do not depend on the injection level and are functions only of z. Equation (5) is much more convenient to use in the determination of (measurable) current than is the standard continuity equation.

III. PHOTOLUMINESCE DECAY RESPONSE

We now apply Eq. (5) to the study of the decay of the excess charge induced by a laser pulse in a semi-infinite (W=∞) sample having constant doping concentration. For low injection minority carriers flow by diffusion and for D independent of z Eq. (5) simplifies to

$$\frac{\partial Q'}{\partial t} = D \frac{\partial^2 Q'}{\partial z^2} - \frac{Q'}{\tau} + G_t(t)(1-R)\alpha\, e^{-\alpha z} \tag{6}$$

where $G_t(t)$ is the total photon flux of the laser beam, R is the reflection coefficient, and α is the absorption coefficient. In (6) the subscript p is dropped for simplicity.

The boundary conditions are

$$Q'(0,z) = 0,\ Q'(t,\infty) = 0,\quad Q'(t,0)S = D \frac{\partial Q'(t,0)}{\partial z} \tag{7}$$

where S is the surface recombination velocity.

If $G_t(t)$ is the unit impulse function, $G_t(t) = \delta(t)$, then Laplace transformation of Eq. (6) with time yields

$$D \frac{\partial^2 Q'(s,z)}{\partial z^2} - \left(s + \frac{1}{\tau}\right) Q' = -(1-R)\alpha\, e^{-\alpha z} \tag{8}$$

where s is the Laplace transform operator. The boundary conditions for Eq. (8) are the Laplace transformation of Eqs. (7). The solution is

$$Q'(s,z) = \frac{\alpha e^{-\alpha z}(1-R)}{-D\alpha^2+s+(1/\tau)} - (\Gamma+\alpha)\alpha\sqrt{D}(1-R)\, \frac{\left[\sqrt{s+(1/\tau)} - \sqrt{D}\,\Gamma\right] e^{-\sqrt{[s+(1/\tau)]/D}\, z}}{\left[-D\alpha^2+s+(1/\tau)\right]\left[s+(1/\tau)-D\Gamma^2\right]} \tag{9}$$

where $\Gamma = S/D$.

If $Q'_t(t)$ the total number of excess carriers and $Q'_t(s)$ its Laplace transformation, then

$$Q'_t(t) = \int_0^\infty Q'(t,z)dz \Rightarrow Q'_t(s) = \int_0^\infty Q'(s,z)dz =$$

$$\frac{1 - R}{-D\alpha^2+s+(1/\tau)} - \frac{(1-R)(\Gamma+\alpha)\alpha D[\sqrt{s+(1/\tau)} - \sqrt{D}\,\Gamma]}{\sqrt{s+(1/\tau)}\,[-D\alpha^2+s+(1/\tau)][s+(1/\tau)-D\Gamma^2]} \cdot \qquad (10)$$

Taking the inverse Laplace transform of Eq. (10), we obtain

$$Q'_t(t) = \frac{\Gamma\alpha(1-R)}{\Gamma-\alpha} e^{-t/\tau}[\frac{1}{\alpha} e^{L^2\alpha^2 t/\tau} \operatorname{erfc}(L\alpha\sqrt{t/\tau}) - \frac{1}{\Gamma} e^{L^2\Gamma^2 t/\tau} \operatorname{erfc}(L\Gamma\sqrt{t/\tau})] \qquad (11)$$

where $L = \sqrt{D\tau}$ is the hole diffusion length. This result holds independently of the beam shape and is the same as Eq. (8) of Ioannou et al [2] derived in the case of a finely focused beam.

If the laser pulse has a flux N(t) that lasts for a finite time T, then the response $Q''_t(t)$ will be the convolution of N(t) with $Q'_t(t)$:

$$Q''_t(t) = \int_0^t N(\tau')\, Q'_t(t-\tau')d\tau' \cdot \qquad (12)$$

If N(T) is a square pulse of amplitude N and width T then, Eq. (12) yields for $t > T$

$$Q''_t(t) = \frac{(1-R)\Gamma\alpha}{\Gamma-\alpha} N \tau e^{-t/\tau} [(L^2\alpha^2-1)^{-1}\alpha^{-1} e^{L^2\alpha^2 t/\tau} \operatorname{erfc}(L\alpha\sqrt{t/\tau}) -$$

$$-e^{T/\tau} e^{L^2\alpha^2(t-T)/\tau} \operatorname{erfc}(L\alpha\sqrt{(t-T)/\tau}) + L((L^2\alpha^2-1)^{-1} - (L^2\Gamma^2-1)^{-1})$$

$$e^{T/\tau}\, e^{(t-T)/\tau}\mathrm{erfc}(\sqrt{(t-T)/\tau}) - e^{t/\tau}\mathrm{erfc}(\sqrt{t/\tau}) + (L^2\Gamma^2-1)^{-1}\Gamma^{-1}$$

$$e^{T/\tau}\, e^{L^2\Gamma^2(t-T)/\tau}\mathrm{erfc}(L\Gamma\sqrt{(t-T)/\tau}) - e^{L^2\Gamma^2 t/\tau}\mathrm{erfc}(L\Gamma\sqrt{t/\tau})\ ] \quad . \qquad (13)$$

If $S = \Gamma = 0$, Eq. (13) reduces to

$$Q''_t(t) = N\,\tau\,(1-R)[e^{T/\tau}-1]\, e^{-t/\tau}, \quad t > T$$

which is a purely exponential function with time constant τ.

As a more general statement, if S=0, the decay of the excess charge will be exponential independently of the shape of the surface at which the sample terminates and independently of the presence of internal fields. This can be proved by integrating the continuity equation,

$$\frac{\partial p'}{\partial t} = -\nabla\cdot\vec{J}_p - \frac{1}{\tau}\,p' \quad ,$$

over the volume of the sample and applying the divergence theorem:

$$\frac{\partial Q'}{\partial t} = -\int_S \vec{J}_p\cdot d\vec{s} - \frac{1}{\tau}\,Q' \quad .$$

Here Q' is the excess minority-carrier charge and the integral above is the hole flux at the surface. This vanishes for S=0. Therefore,

$$\frac{\partial Q'}{\partial t} = -\frac{1}{\tau}\,Q' \quad \text{and} \quad Q' = Q'(0)\, e^{-t/\tau} \quad , \quad t>0 \quad .$$

When $S\neq 0$, eq. (13) implies that $Q''_t(t)$ is not exponential. A measure of the deviation of Q''_t from the exponential function (Constant $\exp(-t/\tau)$ follows from considering the function:

$$\frac{-d[\ln Q''_t(t)]}{dt} = -\frac{dQ''_t/dt}{Q''_t} = \frac{1}{\tau} + \frac{db(t)/dt}{b(t)}$$

where b(t) is the negative of the expression in the square bracket of Eq. (13). The smaller that [db(t)/dt)/b(t)] is the more accurate is the estimation of τ by the slope of $\ln Q''_t$.

One can prove that [db(t)/dt]/b(t) is an increasing function of S and 1/T. As a worst case, we consider infinite recombination velocity and impulse excitation. Then Q''_t becomes:

$$Q''_t = N'(1-R)\, e^{L^2\alpha^2 t/\tau}\, \mathrm{erfc}(L\alpha\sqrt{t/\tau})\, e^{-t/\tau} \qquad (14)$$

where N' is the strength of the pulse. In such a case:

$$\frac{\frac{db(t)}{dt}}{b(t)} = \frac{(1/\sqrt{\pi}) - [L\alpha\sqrt{t/\tau}\, e^{L^2\alpha^2 t/\tau}]\, \mathrm{erfc}(L\alpha\sqrt{t/\tau})}{e^{L^2\alpha^2 t/\tau}\, \mathrm{erfc}(L\alpha\sqrt{t/\tau})} \; \frac{L\alpha\sqrt{t/\tau}}{t} \qquad (15)$$

This is an increasing function of $L\alpha$ and when $L\alpha \to \infty$, then $[db(t)/dt]/b(t) \to 1/2t$. Therefore, in the worst case, by measuring the slope $\ln Q''_t$ at time t, the time constant derived will be $\tau/[1+(\tau/2t)]$ instead of τ. Thus $\tau/2t$ is an upper bound for the percentage error in determining τ. This bound is much lower than the one, 2.47 τ/t, considered by Tyagi et al [2]. Consequently, the maximum error of Dziewior and Schmid [1] due to surface recombination is approximately $\tau/[2(5\tau)] = 10\%$.

If an accuracy of 20% in the recombination lifetime is required, then $0.8 = 1/[1+(\tau/2t)]$ which implies $t=2\tau$. Now the question arises: how can one know when t is equal or greater than 2τ? If $L\alpha\sqrt{t/\tau} > 2$ Eq. (14) can be simplified:

$$Q''_t(t) \simeq Q''_t(0)\ \frac{e^{-t/\tau}}{\sqrt{\pi}L\alpha\sqrt{t/\tau}} \quad . \tag{16}$$

This implies that $Q''_t(2\tau) \simeq 0.05\ Q''_t(0)$ $1/L\alpha$. If L is not known but one can estimate its range, then α can be chosen so that $L\alpha<5$, implying $Q''_t\ (2\tau)>0.01\ Q''_t(0)$. Therefore, by waiting until the response drops to 1% of its initial value, t will be greater than 2τ and the error less than 20%

IV. SUMMARY

The excess charge stored in a sample after laser pulse excitation depends only on the flux of photons of the laser beam. The decay rate of the excess charge is higher than the reciprocal of the bulk lifetime by, at most, a factor $\tau/2t$. This is a result of surface recombination, the associated error of which can be suppressed below 20% by waiting until the response drops to 1% of its initial value when $L\alpha<5$. Thus, in so far as the effects of surface recombination and of uniformity of the incident beam are concerned, photoluminescence decay is a reliable method for determining bulk lifetimes.

ACKNOWLEDGMENTS

This work was supported by the Jet Propulsion Laboratory under Contract No. 956525 and by the National Science Foundation under Grant No. ECS-8203091.

REFERENCES

[1] J. Dziewior, W. Schmid, "Auger coefficient for highly doped and highly excited silicon," Applied Physics Letters, vol. 31, No. 5, 1 Sept. 1977.

[2] D. E. Ioannou, R. J. Gledhill, "Effect of surface recombination on the decay of excess minority carriers in semiconductors induced by finely focused picosecond pulsed laser beam," J. Appl. Phys., 56, (6), 15 Sept. 1984.

[3] M. S. Tyagi, J. F. Nijs, and R. J. Van Overstraeten, "Effect of surface recombination on the transient decay of excess carriers produced by short wavelength laser pulses," Solid State Electronics, 5, pp. 411-415, 1982.

FIGURE CAPTIONS

Figure 1 Schematic illustration of an infinite semiconductor sample bounded by planes z=0, z=W, and excited by a laser beam.

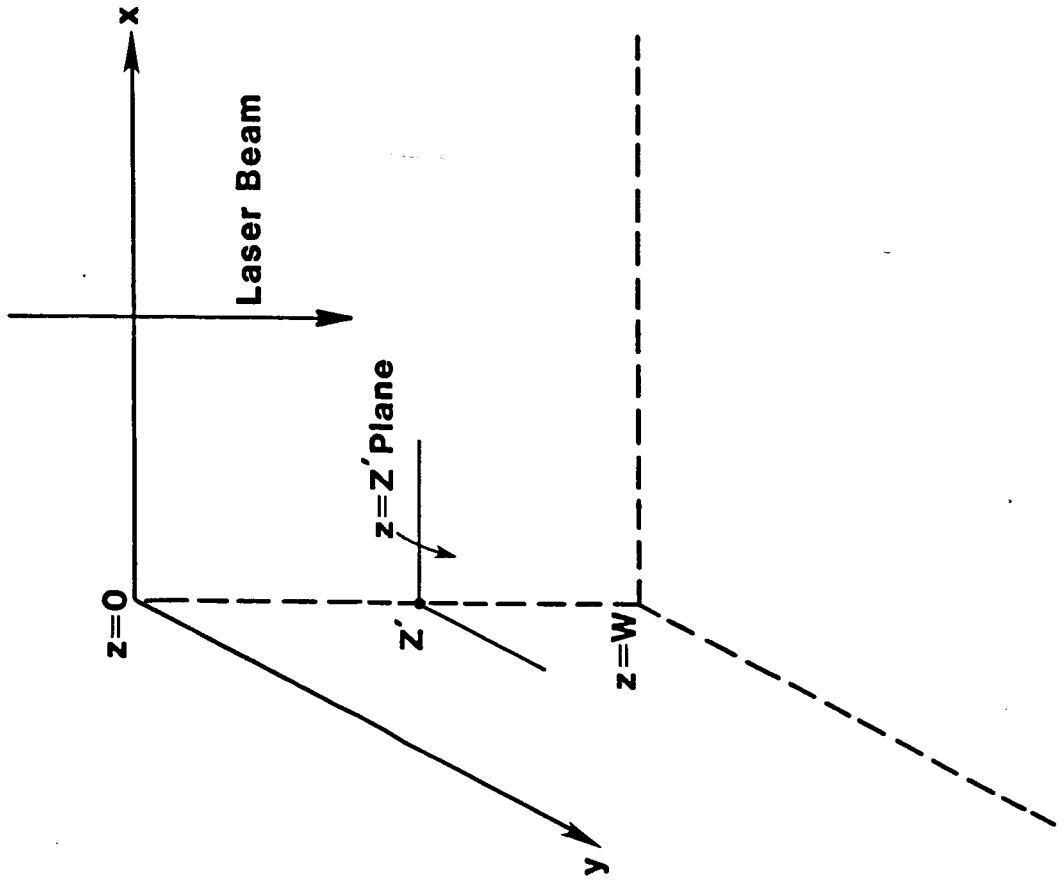
x
Laser Beam
z=Z'Plane
z=0
Z'
z=W
y

CHAPTER FIVE
TRAP CONTROLLED MINORITY-CARRIER MOBILITY IN HEAVILY DOPED SILICON

I. INTRODUCTION

Recently [1], we presented experimental evidence for low diffusivity and mobility of minority holes in highly arsenic doped (concentrations $\sim 10^{20}$ cm^{-3}) n-type Si. This evidence suggests that the minority-carrier diffusivity (and mobility) is about an order of magnitude smaller than the majority-carrier diffusivity in comparably doped p-type Si. As an explanation, we suggested a simple transport model that emphasized trapping by localized tail states in the minority band. The commonly used assumption of an equal minority and majority-carrier mobilities and the neglect of the tail-states effects on the minority-carrier mobility was also questioned in a review article by Abrams et al. [2]. Here we report qualitative evidence that minority-carrier diffusion in n^+ Si may be trap limited.

Figure 1 illustrates the band structure, including the tail states, for n^+ Si. As was already discussed in [1], for low-level injection, the minority holes occupy energy levels near the mobility edge E_V. In the model proposed, the holes from the extended states in the valence band can be captured by the localized tail-states for some mean time $t_{trapping}$, and then released back into the valence band. This process, shown by arrows in the Fig. 1, will decrease the hole mobility. If the scattering rate of holes inside the band is comparable with the hole trapping rate, Sah and Lindholm [3] derive that

$$t_p = et_{coll}/m_p^* \quad , \quad 1/t_{coll} = 1/t_{scatt} + 1/t_{trapping} \quad . \qquad (1)$$

Here t_{coll} is the characteristic collision free time dependent on the mean of the scattering mean free time, t_{scatt}, and the mean trapping time, $t_{trapping}$,

of a minority hole trapped at a bound state energy level E_T, and m_p^* is the effective mass for holes. We investigate the temperature dependence of μ_p by estimating $t_{trapping}$ [3]:

$$1/t_{trapping} \simeq e_p \simeq AT^m \exp\,[-(E_T - E_V)/kT] \qquad (2)$$

where A is a temperature independent constant. In (2) we have assumed, for simplicity, trapping at one shallow level (close to E_V) in the tail band or at an acceptor level in the n^+ region. Such an acceptor level can come from the dopant acceptor (boron in our case) in the p-type substrate of a diffused or ion implanted n^+/p diode. For a parabolic valence band and no degeneracy, m = 2 [3]. However, for band-tail distorted band, the value of m is not known and must be determined experimentally, as is attempted below. At low and high temperatures, respectively, (2) reduces to

$$1/t_{coll}\Big|_{low\ T} \simeq 1/t_{scatt} \quad , \quad 1/t_{coll}\Big|_{high\ T} \simeq 1/t_{trapping} \quad . \qquad (3)$$

Combining (1) and (3), we obtain the trap controlled minority-carrier mobility

$$\mu_{p(trapping)} \simeq [(e/m_p^*)/(AT^m)]\ \exp(E_A/kT) \qquad (4)$$

where $E_A = E_T - E_V > 0$ is the activation energy of the bound-state level E_T.

II. EXPERIMENT AND ANALYSIS

Our experiments provide qualitative support for the hole-trapping model. The experiments involved a measurement of the temperature dependence of the photocurrent response of both n^+/p and p^+/n photodiodes. The

wavelengths of the incident light used create electron-hole pairs almost entirely in the heavily doped n^+ or p^+ region. Transport of photogenerated minority carriers to the collecting p/n junction and the consequent short-circuit current I_{SC} depends on the minority-carrier mobility μ and diffusivity D [4]. Hence I_{SC} and its temperature dependence supplied a vehicle for studying μ nd D.

The devices for which we report findings here were fabricated by arsenic implantation into 5 Ω-cm p-type Si substrates followed by 1200°C anneal for 30 minutes. The resulting n^+ layer was 1.5 μm deep and the sheet resistance was 10 Ω/square. The As concentration was $\sim 10^{20} cm^{-3}$ and nearly independent of position x over about 0.6 μm below the surface (x = 0); for x > 0.6 μm it slowly decreases becoming about $3 \times 10^{19} cm^{-3}$ at 1 μm. The surface was unpassivated, covered only by a thin (~ 10 Å) native oxide layer. Other devices with both unpassivated and SiO_2 passivated surfaces were also studied. The results are similar to those to be presented here. The metal contacts covered less than 10% of the area of the front surface.

The $I_{SC}(T)$ dependence was measured in the wavelength range λ = 0.38 μm to 0.4 μm for which the electron-hole generation rate follows $G(x) = G(0)\exp(-\alpha x)$ [4], where $\alpha > 10^5$ cm^{-1} [5]. Hence contributions of G(x) to I_{SC} originating in the p/n junction space-charge region and in the p-type substrate are negligible. Thus [4]

$$I_{SC} = \frac{AqF(1 - R)}{\alpha D_p} \cdot \frac{\alpha D_p + S_p}{\frac{S_p L_p}{D_p} \sinh\left(\frac{W}{L_p}\right) + \cosh\left(\frac{W}{L_p}\right)} \quad . \tag{5}$$

Here A is the device area, F is the illumination flux density, R is the reflection coefficient, S_p is the effective hole surface recombination velocity, W = 1.3 μm is the thickness of the quasi-neutral n^+ layer, L_p =

$(D_p\tau_p)^{1/2}$ is the hole diffusion length, τ_p is the hole lifetime, and D_p is the hole diffusivity.

The analysis of (5) is complicated if one wishes to obtain the magnitude of the diffusivity D_p or mobility $\mu_p = D_p(kT/q)$ from the measured I_{SC}. In this note we are interested, however, only in a qualitative trends and try to present a simple picture consistent with the data. For this purpose we consider now the temperature dependence of I_{SC}. The temperature dependences of α and R [6] and $\tau_p = \tau_A$ (Auger lifetime) [7] are very small. This leaves S_p and D_p as the only temperature dependent parameters in (5). We neglect the temperature dependence of S_p, for a moment, later justifying this assumption based on experimental results and on theoretical predictions.

Recent measurements indicate that $L_p \simeq 1$ μm in the n^+ silicon doped at about 10^{20} cm^{-3} [8]. Using $W/L_p \simeq 1$ we expand the hyperbolic functions in (5) and set sinh x ≃ cosh x:

$$I_{SC} \simeq B \frac{1}{\alpha S_p} [\alpha D_p + S_p] \tag{6}$$

where $B = AqF(1-R)/W$ is a temperature independent constant. Consider (6) for two special cases. First, if $S_p >> \alpha D_p$, $I_{SC} \simeq B/\alpha$. In this case $I_{SC} \neq f(T)$. This contradicts our experimental result that I_{SC} increases with T (Fig. 2). Thus the second case prevails: $\alpha D_p >> S_p$ (note that $\alpha > 10^5$ cm^{-1}).

To obtain the simple picture, we try the assumption, m=0, and find from (4) and (6) that

$$I_{SC}/T \simeq C \exp(E_A/kT) \tag{7}$$

where C is also nearly temperature independent. From (7), log (I_{SC}/T) vs. $1/T$ is predicted to yield the activation energy $E_A = E_T - E_V$.

On the other hand, if we make the more common assumption of equal majority-and minority-carrier mobilities (and diffusivities), we would then observe

$$I_{SC}/T \simeq C' \tag{8}$$

where in deriving (8) we have used the consistent assumption of near temperature independence of the majority-carrier mobility (hole mobility = 45 cm^2/Vs at T = 20 K; 42 cm^2/Vs at T = 300 K [9]).

The experimental data to follow will decide in favor of (7) rather than (8), implying trap-controlled minority-carrier mobility as opposed to equal minority-and-majority-carrier mobilities.

Figure 2 shows the activation plot of I_{SC}/T versus $1/T$ for two values of F. At low temperature, consistent with our simple model summarized in (7) the inferred mobility depends weakly on T because (in our model) the bound states in the minority band tail have a negligible emission rate and t_{scatt} is a weak function of T. Mobility drops at $T \gtrsim 70$ K (where $t_{scatt} \sim t_{trapping}$) in agreement with (1). For $T \gtrsim 160$ K, μ_p levels off as predicted by (2) for shallow traps. From Fig. 2 we can distinguish two temperature ranges $E_A \simeq$ 10 meV, 70 K < T < 160 K, and $E_A \simeq 2$ meV, T < 70 K.

These activation energies do not have a simple interpretation because of the many levels in the tail. Nevertheless, the value $E_A \simeq 10$ meV and the decrease of μ_p with increasing T are consistent with (2) and (4) of our model for shallow traps with $(E_T - E_V) \lesssim kT$. Moreover, E_A decreases from about 9 meV to about 8.5 meV as F is increased by a factor of five. Increasing F

moves E_{FP} closer to E_V (Fig. 1) which increases the occupation of the tail states closer to E_V and $E_A \simeq (E_T - E_V)/kT$ is expected to decrease, as observed. In the temperature range from about 70 K to about 160 K, where the mobility activation behavior is observed, the variation of the energy gap with T is very small [10], which justifies our assumption of nearly temperature independent α and R [6].

The effect of the temperature variation of the effective surface recombination velocity $S_p(T)$ on $I_{SC}(T)$, which was neglected, is now made credible by the following considerations. First, if $S_p(T)$ is important, E_A is expected to be about $E_G/2 \simeq 0.55$ eV in a Shockely-Read-Hall model even though the surface has distributed states in the energy gap [11]. Second, S_p at the heavily-doped n^+ surface is likely dominated by temperature insensitive Auger effects [11]. Third, results similar to those shown in Fig. 2 were also obtained from the devices for which passivation by SiO_2 sharply decreased S_p.

The fact that I_{SC} is not negligible below $\sim$ 100 K indicates that most of the minority holes are in the extended band states at $T \lesssim 100$ K with only a small fraction trapped at the tail states and immobilized. For the excitations used to measure $I_{SC}(T)$ and also for low-level hole injection in the dark used in [1], the hole concentration in the n^+ region is very small. We can then conjecture that the penetration of the localized tail states into the energy gap is only a very small fraction of the energy gap. This supposition, based on our data, agrees with recent theoretical calculations of the band structure of heavily doped Si [12].

It follows directly from our trapping model that μ(minority) < μ(majority) could apply also in the absence of the tail states because shallow impurity levels can act as traps near the minority-band edge (Fig. 1). This suggests that μ(minority) may strongly depend on compensation. A lack of

compensation in their epitaxial p/n diodes may be responsible for the experimental observation by Dziewior and Silber [13] that μ(minority) $\simeq$ μ(majority) for concentration in Si $< 10^{19}$ cm^{-3}.

Although the assumptions needed to derive (7) from (5) introduce some inaccuracy in the model for the activation energy of minority-carrier mobility (diffusivity), the general conclusions derived by comparing (7) with the experimental trends exhibited in Fig. 2 are anticipated to remain valid. The exact value of the activation energy in a single-trap model remains in question. When more detailed knowledge concerning the values and the temperature dependencies of parameters in (5) become available, one can then use data presented here to explore aspects of the minority-carrier band tail.

The purpose here is less ambitious. We have demonstrated activation behavior of the minority-carrier mobility and diffusivity, exhibiting thereby an activation energy of the order of kT (for 300 K) as one expects for the prominently active tail states. Moreover, our data in Fig. 2, as interpreted here, supports the inadequacy of the commonly used assumption of equal majority- and-minority-carrier mobilities; in turn, this supports interpretations, such as that in [1], of larger values of energy-gap narrowing than is common in the literature.

Lastly, we point out that the assumed value, $m \simeq 0$, and values $m < 0$ in (4) are self-consistent with the experimental results of Fig. 2, but values $m > 0$ are not. However, regardless of the value of m, the $I_{SC}T^m$ vs. 1/T plot shows an activation behavior, thus the assumption of μ(majority) = μ(minority) is always wrong (see Eq. 8).

This work was supported in part by National Science Foundation Grant ECS-8203091 (A.N.), Solar Energy Research Institute Contract No. XB-3-02090-2 (F.A.L., A.N.), and Jet Propulsion Laboratory (C.T.S.). We acknowledge useful discussions with Peter T. Landsberg.

REFERENCES

1. A. Neugroschel, S.C. Pao, and F.A. Lindholm, IEEE Trans. Electron Devices, ED-29, 894 (1982).

2. R. A. Abram, G. J. Rees and B. L. H. Wilson, Adv. Phys., 27, 799 (1978).

3. C.T. Sah and F.A. Lindholm, Solid-State Electron., 16, 1447 (1973).

4. H.J. Hovel, Solar Cells, (Academic Press, New York, 1975).

5. G. Lubberts and B.C. Burkey, J. Appl. Phys. 55, 760 (1983).

6. W.C. Dash and R. Newman, Phys. Rev. 99, 1151 (1955).

7. J. Dziewior and W. Schmid, Appl. Phys. Lett., 31, 346 (1977).

8. G. E. Possin, M. S. Adler, B. J. Baliga, IEEE Trans. Electron Devices, ED-31, 3 (1984).

9. C.T. Sah, P.C.H. Chan, C.K. Wang, R.C.Y. Sah, K.A. Yamakawa, and R. Lutwak, IEEE Trans. Electron Devices, ED-28, 304 (1981).

10. See, for example, S. M. Sze, Physics of Semiconductor Devices, Wiley 1969, p. 24.

11. P.T. Landsberg and M.S. Abrahams, Solid State Electron., 26, 841 (1983).

12. A. Selloni and S.T. Pantelides, Phys. Rev. Lett., 49, 586 (1982).

13. J. Dziewior and D. Silber, Appl. Phys. Lett., 35, 170 (1979).

FIGURE CAPTIONS

Fig. 1. Qualitative illustration of the band edges of heavily doped n^+-silicon. The broken lines show the unperturbed parabolic bands. The positions of both the electron and hole quasi-Fermi levels is also indicated. The arrows near E_V indicate hole capture and emission by the tail states and by the acceptor level from the p-type substrate. The penetration of the tail states into the forbidden gap is assumed to be very small in comparison with the bandgap $E_G = E_C - E_V$.

Fig. 2. Normalized short-circuit photocurrent versus 1/T for $\lambda = 0.4$ μm. The illumination density for curve 1 is five times larger compared to that of curve 2.

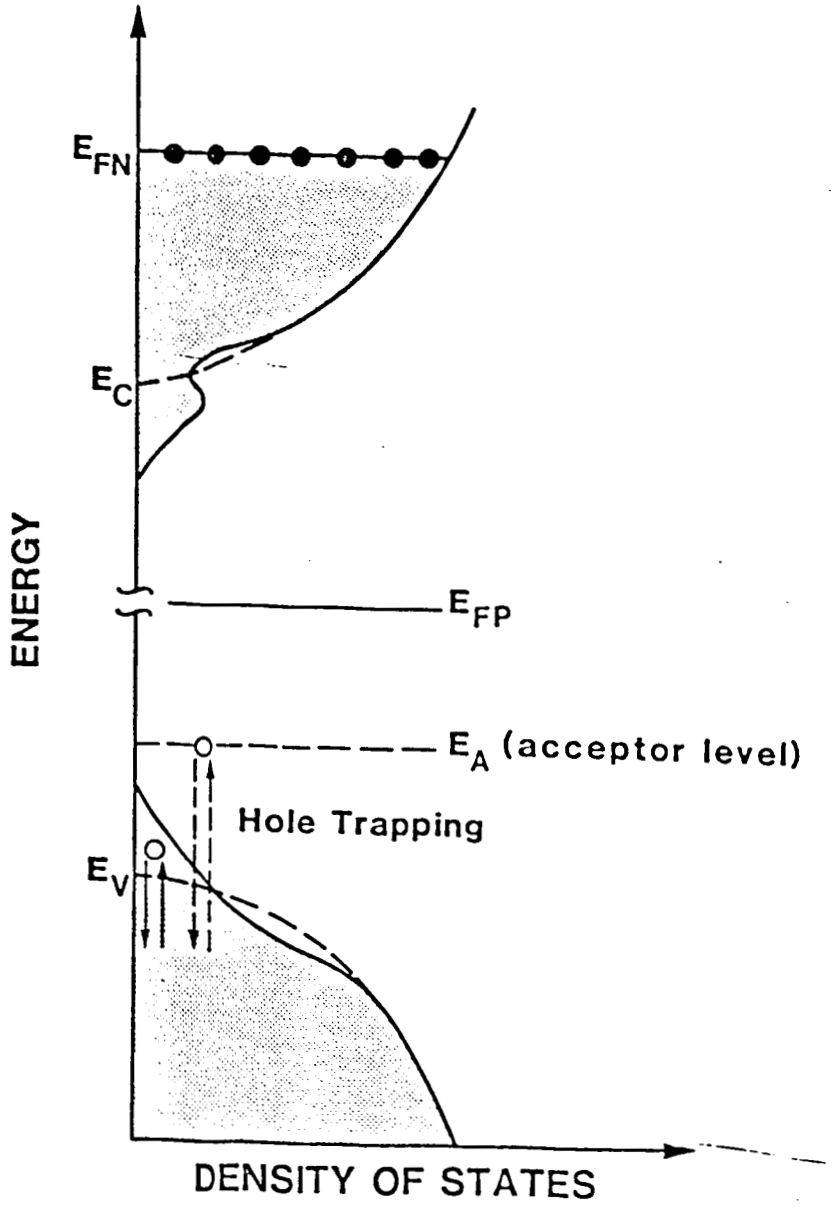
E_{FN}
E_C
ENERGY
E_{FP}
E_A (acceptor level)
Hole Trapping
E_V
DENSITY OF STATES

Fig. 1

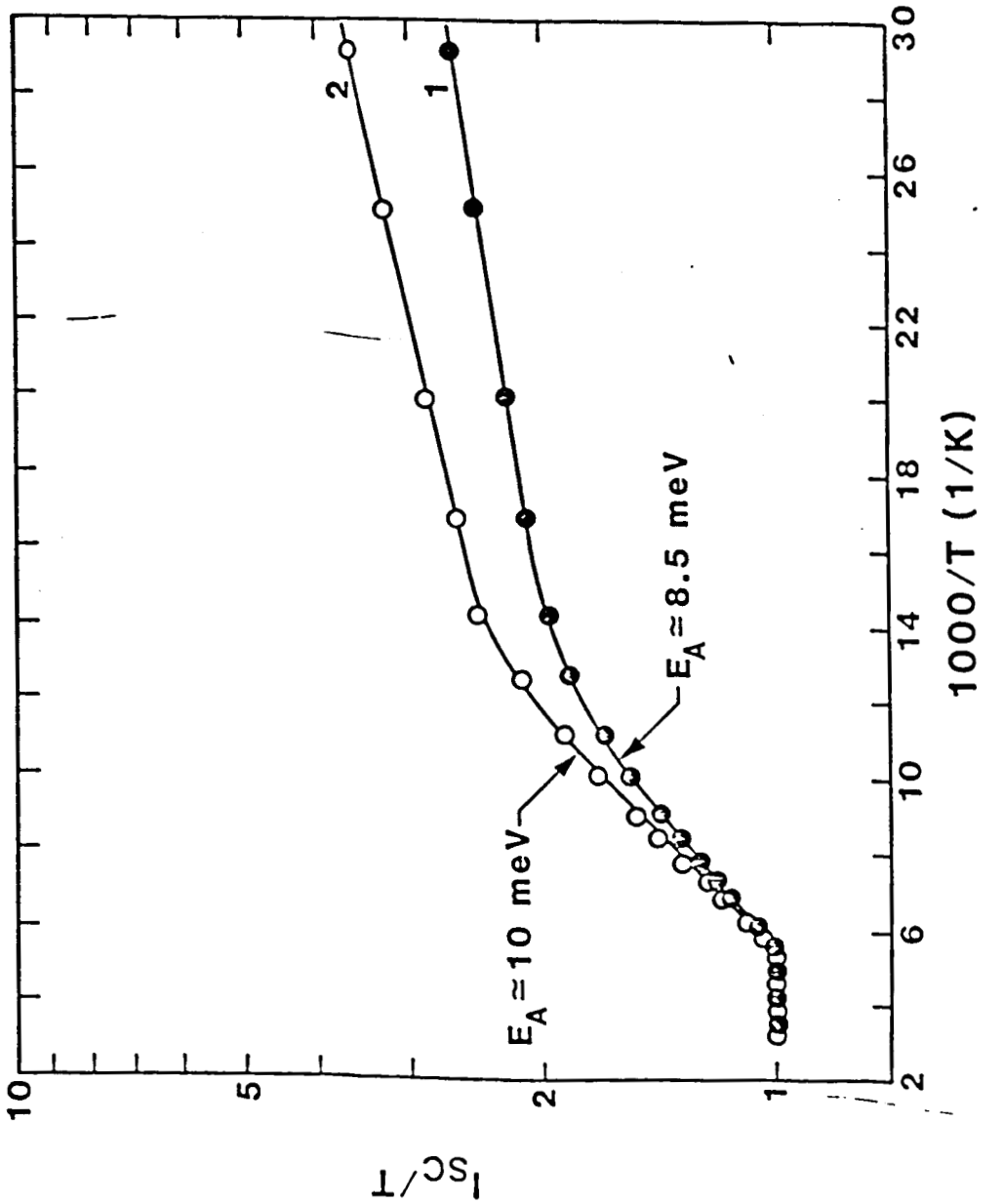
I_{SC}/T
10
5
2
1
2
1
$E_A \cong 10$ meV
$E_A \cong 8.5$ meV
2
6
10
14
18
22
26
30
1000/T (1/K)

Fig. 2

CHAPTER SIX
DETAILED INTERPRETATION OF PHOTOCONDUCTIVITY DECAY RESPONSE FOR LIFETIME DETERMINATION

Our purpose here is to clarify the relation between the observed transient photoconductive decay and a previous development of the detailed physics [1] underlying this transient.

To make this clarification concrete, we begin with a review of the work of Othmer and co-workers, who compared photoconductivity-decay lifetime with steady-state lifetime for silicon [2]. Figure 1 reproduces this comparison. The steady-state lifetime was measured by steady-state photoconductivity and the transient lifetime was measured by transient photoconductivity. By introducing various impurities (Zr, Mn, Mg, Ni, and V) known to produce recombination centers in Si and by varying the concentrations of these impurities, Othmer and co-workers varied the steady-state lifetime. Note the scatter of the data. Note also the large number of data points yielding a photoconductivity decay lifetime considerably more than a factor of two greater than the steady-state lifetime.

From Othmer's results we see that the photoconductivity decay is characterized by an apparent single characteristic time; yet this characteristic time differs considerably from the steady-state lifetime.

To suggest an explanation for this apparent anomaly, we review briefly some aspects of our prevous theoretical work on fast photoconductive switches, which we have called photoconductive circuit elements [1]. In these devices, incident light creates hole-electron pairs in very high injection in a nearly intrinsic region of a p/i/n or n/i/n or p/i/p photoconductor. Though a combination of a Dember field and a high surface recombination velocity causes a peak in the hole and electron density in the y direction normal to the surface on which the light shines [3], integration of the continuity equation

in the y direction leads one to analyze a related device having no dependence of variables in the y direction in the active region. (This approach resembles that used in MOSFET theory to reduce the number of space variables required.)

Then, provided the injection level is high enough that the particle dielectric relaxation time is much less than the drift transit time in the x direction resulting from an applied electric field, the device is in a quasi-neutral condition [1]. Thus the turn-off transient becomes a problem in quasi-neutral photoconductive decay in the simplest model: that in which the x or y coordinates do not enter.

Despite this reduction to a simple model, some complexities arise from recombination through many traps--a prominent feature of this class of photoconductive device [1]. For example, for incremental variations in the particle electrochemical potentials, variations that are much smaller than a thermal voltage, a detailed description of decay involves two characteristic times for each participating bound state in the forbidden band. This contrasts with the single characteristic time, the high-level recombination lifetime, that prevails for the time-invariant steady state. Note that these multiple characteristic times apply only for incremental times. In Ref. 1, apparently the first method is developed for determining **large-signal** transient that incorporates these multiple time constants.

For the recombination parameters indicated in Fig. 2, we compare the 1/e fall time calculated by this method with that resulting from the standard steady-state lifetime, a single-level Shockley-Read-Hall mechanism. From this comparison we see two key results. First, the single-lifetime calculation underestimates the 1/e fall time by about a factor of 1.5 in this example. This effect results from the trap readjustment time [1], which is neglected in

the standard single-lifetime model. Second, the net effect of two characteristic times, which exist for incremental times, yields an essentially **single-exponential** decay for the **large-signal** response.

The combination of these two results suggest an interpretation of the data of Fig. 1 different from that advanced by Othmer and co-workers [2]. We suggest that the observation of photoconductive decay exhibiting an apparent **single** characteristic time that differs considerably from the steady-state lifetime is not an anomaly. Rather this results directly from the underlying physics of photoconductive decay for samples having a large density of recombination centers.

This physics has several features. First, for incremental times and small-signal responses, as defined above, two characteristic times are needed for each recombination-center level to describe fully the transient decay. This detail of the physics was first advanced by Sandiford [4] and later was extended by Sah [5]. Second, the incremental decay response can be used to yield the large-signal decay response. A method for doing this appears in Ref. 1. Third, the large-signal response has an apparent single characteristic time (which exceeds the steady-state lifetime) that prevails over several decades of decay of the excess carrier densities. This third feature was overlooked in Ref. 1, and apparently has not appeared previously. It provides a key to the detailed interpretation of photoconductive-decay experiments.

We acknowledge the support of the Silicon Solar Array Project of the Jet Propulsion Laboratory, California Institute of Technology, in conjunction with NASA and DOE. We thank Bob Hammond and C. Tang Sah for help on technical aspects of this and related work.

REFERENCES

1. B. Y. Hwang, F. A. Lindholm and R. B. Hammond, "Methodology for calculating turn-off transient of photoconductive circuit elements in picosecond optoelectronics," IEEE J. Quantum Electron., vol. QE-19, pp. 648-657, Apr. 1983.

2. S. Othmer and S. C. Chen, "Characterization of nonideal silicon in terms of lifetime and diffusion length," in 14th IEEE Photovoltaic Specialists Conf., pp. 1238-1243, 1978.

3. B. Y. Hwang and F. A. Lindholm, "Dember effect in fast photoconductive circuit elements," IEEE Electron Devices, vol. ED-31, pp. 101-104, 1984.

4. D. J. Sandiford, "Carrier lifetime in semiconductors for transient conditions," Phys. Rev., vol. 105, p. 524, 1957.

5. C. T. Sah, "The equivalent circuit model in solid-state electronics, Part I: The single energy level defect centers," Proc. IEEE, vol. 55, pp. 654-671, 1967.

FIGURE CAPTIONS

Fig. 1 Comparison of photoconductivity decay lifetime measured by Westinghouse and steady-state lifetime measured by Northrop on symbols derived from the same ingots [2].

Fig. 2 Comparison of decay times for capture rates (thermal velocity times capture cross section) $c_n = c_p = 10^{-8}$ cm^3/s, $N_{TT} = 10^{18}$ cm^3. Curve (a), calculated by using two transient time constants, contrasts with curve (b), calculated using a model based on a single steady-state lifetime. The 1/e decay time is 1.5 times longer than that predicted by a single steady-state lifetime for the parameters chosen. This theoretical dependence, for InP, will scale properly, for example, for Si, where a capture cross section of 10^{-15} cm^{-3} and a thermal velocity of 10^6 cm/s (> 10^7 cm/s for electrons in InP) and a flaw density of 10^{15} will yield $\tau = 1$ μs.

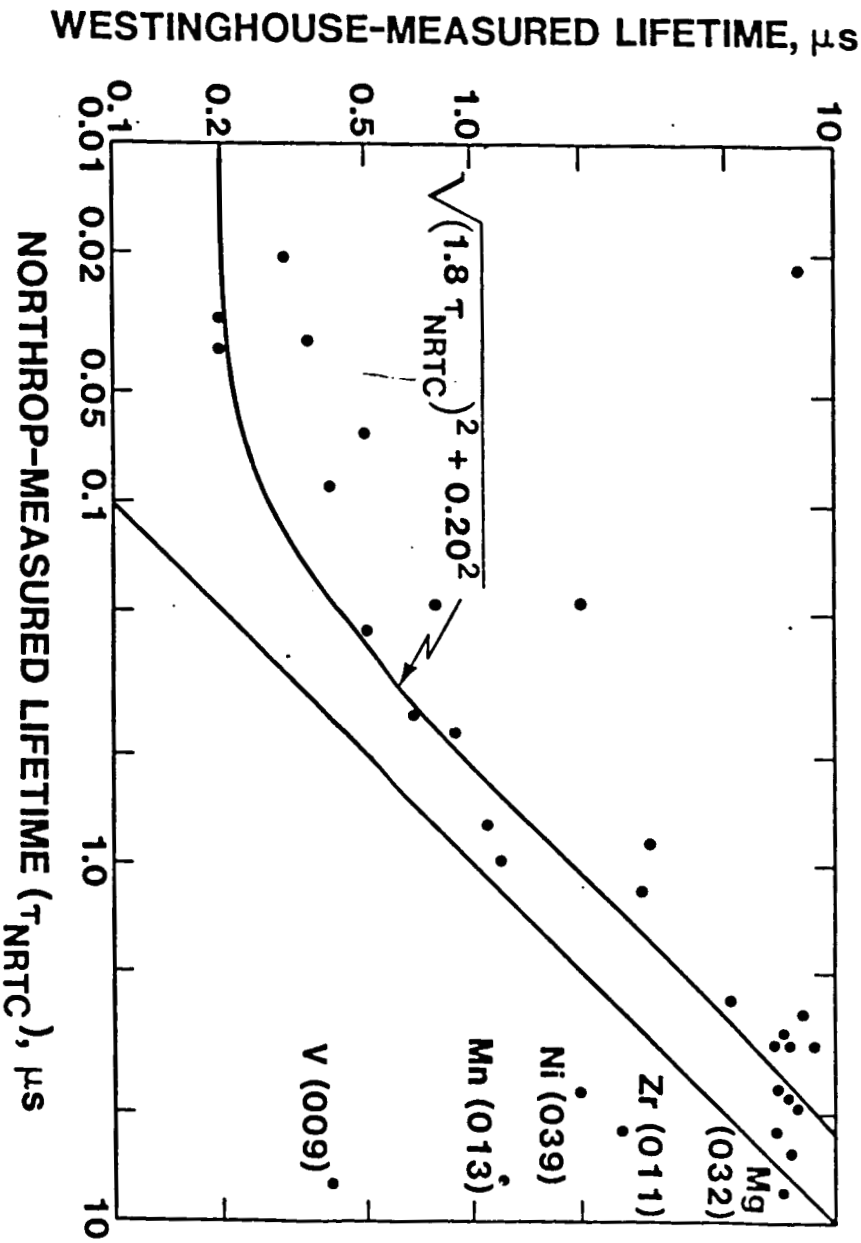
WESTINGHOUSE-MEASURED LIFETIME, μs
NORTHROP-MEASURED LIFETIME (τ_{NRTC}), μs
0.1
0.01
0.02
0.05
0.1
0.2
0.5
1.0
10
$\sqrt{(1.8\ \tau_{NRTC})^2 + 0.20^2}$
Mg (032)
Zr (011)
Ni (039)
Mn (013)
V (009)

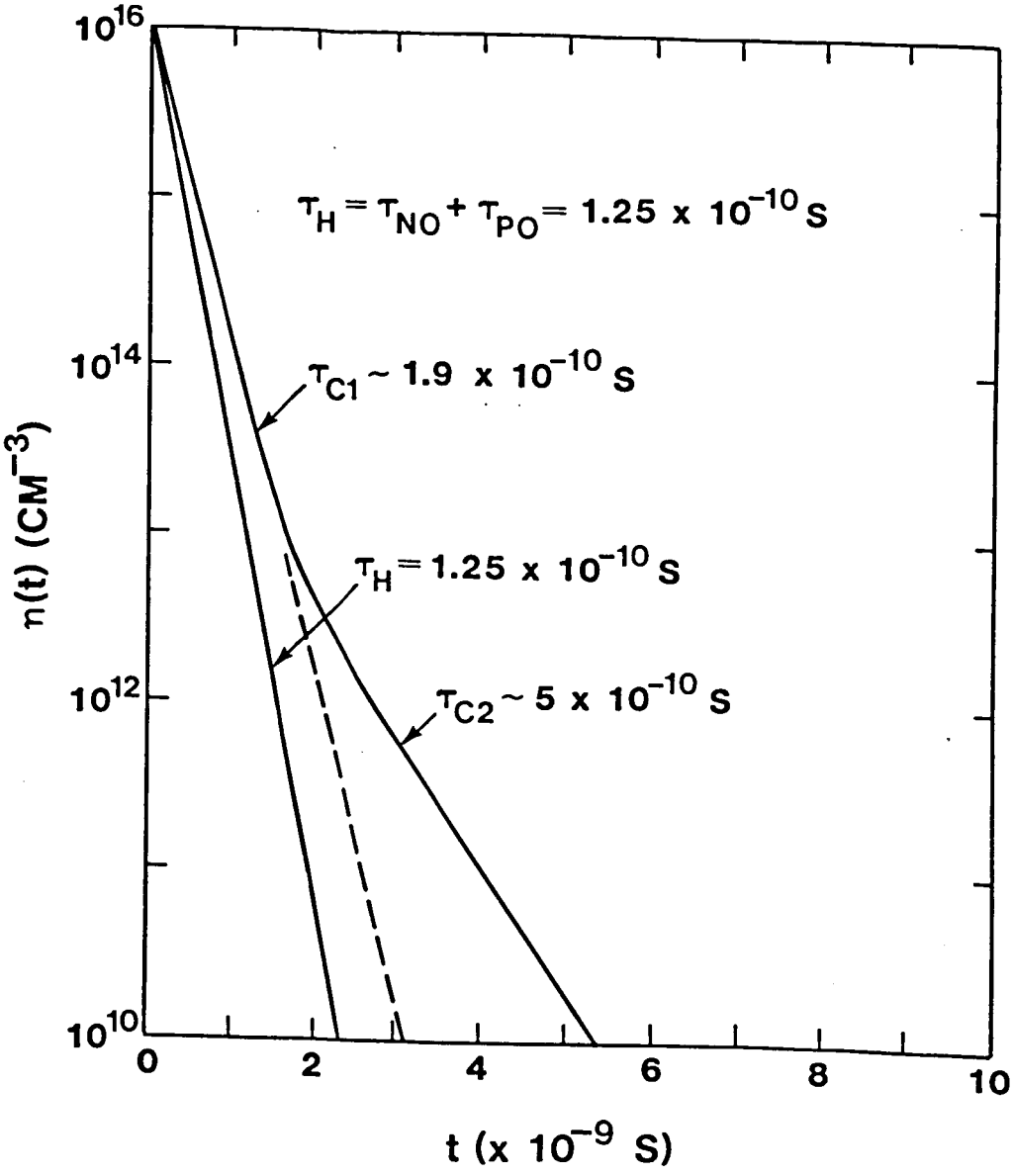
10^{16}
10^{14}
10^{12}
10^{10}
$n(t)\ (CM^{-3})$
$\tau_H = \tau_{NO} + \tau_{PO} = 1.25 \times 10^{-10}\ S$
$\tau_{C1} \sim 1.9 \times 10^{-10}\ S$
$\tau_H = 1.25 \times 10^{-10}\ S$
$\tau_{C2} \sim 5 \times 10^{-10}\ S$
0
2
4
6
8
10
$t\ (\times 10^{-9}\ S)$

CHAPTER SEVEN
GENERALIZED RECIPROCITY THEOREM FOR SEMICONDUCTOR DEVICES

In a recent paper, Donolato[1] has proven a version of the reciprocity theorem for the charge collection by a p-n junction in the presence of a unit point generation source. The proof was restricted to a uniform material in which only the lifetime was allowed to vary with position. We extend this proof to p-n junction devices having three-dimensional space dependencies of all material parameters. In addition, we prove that reciprocity holds also for transients and state another form of reciprocity relating quasi-Fermi levels and point generation in a quasineutral region under low injection conditions.

The conventional reciprocity theorem relating input voltages and output currents in the base of a transistor was proven by W. Shockley et al.[2] in one of the early papers on p-n junction transistors. In this letter we generalize Shockley's procedure in order to prove reciprocity for charge collection.

The principal quasineutral region of the diode, where carrier generation and recombination takes place, is bounded by the junction S_J and the rest of the surface S_L (lateral and back surface) characterized by a position dependent surface recombination velocity s'. The region is assumed to be p-type in low injection. Extension to n-type regions is straightforward. Two different excitation cases are considered. In case 1 the junction is forward biased by a voltage V in the dark. In case 2 the junction is short circuited and a point generation source of strength G is applied at point $\mathbf{r}'$. If J, n and J',n' are the minority (electron) current density and excess minority carrier concentration for cases 1 and 2 respectively, then the boundary conditions for each case are

$$\frac{n(\mathbf{r}_J)}{n_o(\mathbf{r}_J)} = \exp\left(\frac{qV}{kT}\right) - 1 \quad , \quad n'(\mathbf{r}_J) = 0 \quad , \tag{1}$$

where r_J is a point on the junction edge S_J and n_o is the equilibrium minority carrier concentration. The continuity equation for cases 1 and 2 is

$$-\frac{1}{q}\nabla\cdot\mathbf{J} = -\frac{n}{\tau} \quad , \quad -\frac{1}{q}\nabla\cdot\mathbf{J}' = -\frac{n'}{\tau} + G\,\delta(\mathbf{r}-\mathbf{r}') \tag{2}$$

where $\delta(\mathbf{r}-\mathbf{r}')$ represents a unit point carrier generation source applied at $\mathbf{r}=\mathbf{r}'$, and τ is the lifetime. Because of low injection, the electric field E, the mobility μ and the lifetime τ are independent of the excitation. The system is linear.

Let vector A be defined by the equation

$$\mathbf{A} = \frac{n}{n_o}\mathbf{J}' - \frac{n'}{n_o}\mathbf{J} \quad . \tag{3}$$

The surface integral $\int_{S_L} \mathbf{A}\cdot d\mathbf{s}$ vanishes since on S_L

$$\mathbf{A}\cdot d\mathbf{s} = -q\left(\frac{nn'}{n_o}s' - \frac{n'n}{n_o}s'\right) = 0 \quad . \tag{4}$$

From Eq. (1) this integral on S_J becomes

$$\int_{S_J} \mathbf{A}\cdot d\mathbf{s} = \left[\exp\left(\frac{qV}{kT}\right) - 1\right] \int_{S_J} \mathbf{J}'\cdot d\mathbf{s} = \left[\exp\left(\frac{qV}{kT}\right) - 1\right] I' \tag{5}$$

where I' is the current due to the point source exiting the p-type region through the junction. Therefore, if S is the entire surface enclosing the quasineutral region, then from Eqs. (4), (5) the total surface integral of A becomes

$$\int_S \mathbf{A}\cdot d\mathbf{s} = \int_{S_L} \mathbf{A}\cdot d\mathbf{s} + \int_{S_J} \mathbf{A}\cdot d\mathbf{s} = \left[\exp\left(\frac{qV}{kT}\right) - 1\right] I' \quad . \tag{6}$$

By using Eq. (2), the Einstein relationship for non-degenerate minority carriers, $D = (kT/q)\mu$, and the expression for the electric field $E = -(kT/q)\nabla \ln n_o$, the divergence of A can be written as

$$\nabla\cdot\mathbf{A} = \nabla\cdot\left[\frac{n}{n_o}\mathbf{J}'\right] - \nabla\cdot\left[\frac{n'}{n_o}\mathbf{J}\right] = \frac{1}{n_o}[\nabla n - n\nabla \ln n_o]\cdot\mathbf{J}' +$$

$$\frac{n}{n_o}\nabla\cdot\mathbf{J}' - \frac{1}{n_o}[\nabla n' - n'\nabla \ln n_o]\cdot\mathbf{J} - \frac{n'}{n_o}\nabla\cdot\mathbf{J} =$$

$$\frac{1}{n_o}[\nabla n + \frac{q}{kT}n\mathbf{E}]\cdot[q\mu n'\mathbf{E} + qD\nabla n'] - q\frac{n}{n_o}\left[-\frac{n'}{\tau} + G\,\delta(\mathbf{r}-\mathbf{r}')\right]$$

$$-\frac{1}{n_o}[\nabla n' + \frac{q}{kT}n'\mathbf{E}]\cdot[q\mu n\mathbf{E} + qD\nabla n] + q\frac{n'}{n_o}\left[-\frac{n}{\tau}\right] =$$

$$\frac{1}{n_o}\mu kT[\nabla n + \frac{q}{kT}n\mathbf{E}]\cdot[\frac{q}{kT}n'\mathbf{E} + \nabla n'] + q\frac{nn'}{n_o\tau} - q\frac{n}{n_o}G\,\delta(\mathbf{r}-\mathbf{r}')$$

$$-\frac{1}{n_o}\mu kT[\nabla n' + \frac{q}{kT}n'\mathbf{E}]\cdot[\frac{q}{kT}n\mathbf{E} + \nabla n] - q\frac{n'n}{n_o\tau} = -q\frac{n}{n_o}G\,\delta(\mathbf{r}-\mathbf{r}') \quad . \qquad (7)$$

By using Guass' theorem and from Eqs. (6) and (7)

$$\int_S \mathbf{A}\cdot d\mathbf{s} = \int_V \nabla\cdot\mathbf{A}\,dv \Rightarrow [\exp(\frac{qV}{kT}) - 1]I' =$$

$$-q\int_V \frac{n}{n_o}G\,\delta(\mathbf{r}-\mathbf{r}')dv = -q\frac{n(\mathbf{r}')}{n_o(\mathbf{r}')}G \quad . \qquad (8)$$

Equation (8) is similar to Donolato's final expression. It is more general because we include position dependencies of μ, D and $n_o(x)$.

We introduce the minority carrier quasi-Fermi level in dark, F_n, referenced to the majority carrier Fermi level, which is assumed position independent[3]. Then, Eq. (8) becomes

$$I' = - q \frac{\exp(F_n(\mathbf{r}')/kT) - 1}{\exp(qV/kT) - 1} G \neq f(V) \qquad (9)$$

because of linearity. Thus we can choose V conveniently so that $\exp(qV/kT) - 1 = 1$. Then Eq. (9) becomes

$$I' = - q [\exp(F_n(\mathbf{r}')/kT) - 1] G \quad . \qquad (10)$$

Equation (10) expresses that the probablility of collection of a minority carrier generated at point $\mathbf{r}'$ is $\exp(F_n(\mathbf{r}')/kT) - 1$.

In a similar manner, one could prove another form of the reciprocity theorem applying to a quasineutral region in low injection: the minority-carrier quasi-Fermi level at point 1 due to a point source applied at point 2 is the same as the minority-carrier quasi-Fermi level at point 2 due to the same source applied at point 1.

These theorems hold also for transients. This is proved by replacing n,I and n',I' by their Laplace transforms and by transforming the continuity equations for zero initial conditions:

$$\frac{\partial n}{\partial t} = \frac{1}{q} \nabla \cdot \mathbf{J} - \frac{n}{\tau} \Rightarrow sn(s) = \frac{1}{q} \nabla \cdot \mathbf{J}(s) - \frac{n(s)}{\tau} \Rightarrow$$

$$-\frac{1}{q}\nabla\cdot\mathbf{J}(s) = -\left(s + \frac{1}{\tau}\right)n(s) \quad , \tag{11a}$$

$$\frac{\partial n'}{\partial t} = \frac{1}{q}\nabla\cdot\mathbf{J}' - \frac{n'}{\tau} + G\,\delta(\mathbf{r} - \mathbf{r}') \Rightarrow$$

$$-\frac{1}{q}\nabla\cdot\mathbf{J}'(s) = -\left(s + \frac{1}{\tau}\right)n(s) + G(s)\delta(\mathbf{r} - \mathbf{r}') \tag{11b}$$

Substitution of Eq. (11) into (7) and (8) will give the same result as in the steady state.

Equation (10) could be useful in solar cell theory since it allows the calculation of short-circuit current from the analysis of the device under dark conditions:

$$I_{SC} = \sum_{i=1,2} (-q) \int_i \left[\exp(F_m(\mathbf{r})/kT) - 1\right] G(\mathbf{r})d^3\mathbf{r} \quad , \tag{12}$$

where 1,2 represent the quasineutral emitter and base of the cell, F_m is the minority carrier quasi-Fermi level in <u>each</u> region in dark and under bias V such that $\exp(qV/kT) - 1 = 1$ and G is the generation rate. Equation (12) holds under the same assumptions underlying the proof of the reciprocity theorem and ignores generation in the space charge region.

The major assumption in deriving Eq. (8) was low level injection so that the system could be treated as linear. Low injection guarantees linearity of the system even in the presence of the effects of heavy doping or graded chemical composition. In this case, in the equation $-\nabla \ln n_o = qE/kT$, E will be the minority carrier field which includes the quasi-fields arising from the position dependent energy gap electron affinity and density of states.

Therefore, the original Shockley's proof of reciprocity can be extended to heavily doped three dimensional base regions to obtain relations between input voltages and output currents. In this sense, Shockley's proof is more general than the recently published[4] proof of reciprocity in one- dimensional transistor base regions which takes into account heavy doping effects.

The practical significance of reciprocity is that it can reduce the number of unknowns in a problem and reduce the amount of calculations needed. As an example, in the recent paper by del Alamo and Swanson[3], the quantum efficiency of an emitter could have been found by integrating Eq. (10), since the minority carrier Fermi level as a function of position was already numerically calculated under dark conditions. In addition, their forward and reverse transport factors and saturation currents are related by the relation $\alpha_f J_{of} = \alpha_r J_{or}$. Thus the present reciprocity theorem can find use in the measurement of such device parameters as the surface recombination velocity at a polycrystalline silicon contact.

Although not discussed here, reciprocity relations enter the physics of many different phenomena, such as heat conduction or thermoelectric effect. These relations are based on fundamental considerations relating to detailed balance under thermal equilibrium and Onsager's principle of microscopic reversibility.

ACKNOWLEDGMENTS

This work was supported in part, by the Jet Propulsion Laboratory and Motorola, Inc.

REFERENCES

[1] C. Donolato, Appl. Phys. Lett. **46**, 270 (1985).

[2] W. Shockley, M. Sparks and G. K. Teal, Phys. Rev. **83**, 151 (1951).

[3] J. A. del Alamo and R. M. Swanson, IEEE Trans. Electron Devices **ED-31**, 1878 (1984).

[4] H. J. De Man, M. Y. Ghannam, and R. P. Mertens, IEEE Trans. Electron Devices **ED-31**, 1720 (1984).

CHAPTER EIGHT
MINORITY-CARRIER DIFFUSION COEFFICIENTS AND MOBILITIES IN SILICON

Minority-carrier mobility is one of the principal parameters determining the transport properties of minority carriers in p-n junction devices. The majority-carrier mobility (conductivity mobility) is important for determination of the resistance of semiconductor regions. Accurate data and theoretical expressions for the conductivity mobility in both the n- and p-type Si are available [1-6]. Only very limited date are presently available for the minority carriers. Prince [7] measured the minority-carrier drift mobilities of electrons μ_n and holes μ_p using the Haynes-Shockley pulse method. Dannhauser [8] and Krausse [9] measured the sum $(\mu_n + \mu_p)$ from an ohmic drop of forward-biased p-i-n diodes. Recently, Dziewior and Silber [10] determined the minority-carrier diffusion coefficients, $D = (kT/q)\mu$,in the doping range from about 10^{17} cm^{-3} to about 10^{19} cm^{-3} by measuring the complex diffusion length of the minority carriers generated by 10.7 MHz optical excitation. These recent data show good agreement with the conductivity electron mobility, but the hole mobility in n-type Si was up to ~30% higher than the hole conductivity mobility in p-type Si. Burk and de la Torre [11] confirmed the result of [10] for one value of doping ($N_{DD} = 2.6 \times 10^{18}$ cm^{-3}). In contrast to the results of [10], the measurements of Prince [7] show that both μ_n and μ_p are smaller than the majority carrier values. Some possible reasons for the discrepancies are discussed in [10]. Additional reasons may be due to the insufficient purity of Si crystals used in 1954 by Prince [7].

Because of the scarcity of the accurate and reliable values for minority-carrier mobilities and because of discrepancies among the results quoted above, modeling of p-n junction devices is based on a convenient assumption of

equal minority and majority carrier mobilities. In addition to [10], several other theoretical [12-14] and experimental [15,16] works suggested that the above assumption is not valid, particularly in heavily doped Si. To verify this assumption, we present a new and accurate method for measurement of the minority-carrier diffusion coefficients in semiconductors. The method is applicable for both low and highly doped materials and is demonstrated here for low doped Si.

The present method is based on a direct measurement of the transit time of the minority carriers through a narrow region of a p-n diode. Assume a p^+-n diode in which the hole diffusion length $L_p \gtrsim W$, where W is the width of the n-base region terminated by an ohmic contact with recombination velocity S. As was shown by Gonzalez and Neugroschel [17], the real part of the small-signal hole admittance for frequencies $\omega \gtrsim 10/\tau_p$ follows the $\omega^{1/2}$ dependence according to

$$G_p^{HF} = K(D_p/L_p)(\omega\tau_p/2)^{1/2} \tag{1}$$

where $K = (q/kT)(qA\, n_i^2/N_{DD})\, \exp[(qV/kT) - 1]$ is a constant depending on device area A, base doping density N_{DD}, temperature $n_i^2(T)$, and applied voltage V, and $\tau_p = (L_p^2/D_p)$ is the hole lifetime. The extrapolation of this dependence to the low-frequency value for large S_p given by the standard relation $G_p^{LF} = K(D_p/L_p)\coth(W/L_p)$ gives an intercept at

$$\omega_I = (2D_p/L_p^2)\coth^2(W/L_p)\,. \tag{2}$$

This can be further simplified for $(W/L_p) \lesssim 0.3$ as

$$\omega_I = 2D_p/W^2 = 1/\tau_t \qquad (3)$$

where $\tau_t = W^2/2D_p$ is the transit time across the base.

Equations (2) and (3) are the basis of the method proposed. The method requires the measurement of only one parameter G_p^{HF}, and is applicable for any narrow region with known value W, regardless of doping.

To demonstrate the method, we show in Fig. 1 the measured and theoretical dependencies of G_p vs frequency $f = \omega/2\pi$ for a p^+-n device with $N_{DD} = 7.25 \times 10^{14}$ cm^{-3} and W = 310 μm. The intercept frequency is $f_I = 6.59$ kHz. To obtain D_p we use (2) with accurately measured [17-19] $L_p = 500 \pm 10$ μm and obtain $D_p = 15.71 \pm 1$ cm^2/s and $\mu_p = 608 \pm 40$ cm^2/Vs at T = 300 K. This value for the mobility is about 30% higher than the majority-carrier value of 470 cm^2/Vs [2]. The error of about ± 40 cm^2/Vs is an estimated total experimental accuracy which is discussed in more detail below.

The error in using (2) instead of (3) is very small. For example, a 10% error in L_p for the sample in Fig. 1 yields less than 1% error in D_p. The error can be eliminated by using thinner samples as shown later. In obtaining the above result from the measured conductance we assumed a negligible contribution of the p^+-emitter to the conductance. This can be justified by noting that the intersect frequency corresponding to the emitter transit time t_{tE} is $f_{IE} = (1/2\pi)(1/t_{tE}) = (1/2\pi)(2D_n/W_E^2) \simeq 10^9$ Hz for $W_E \simeq 0.2$ μm and $D_n \sim 1$ cm^2/s, which is much smaller than the observed base $f_{IB} \simeq 6$ kHz in Fig. 1. Note also a small hump at the knee in Fig. 1, which is characteristic of the base and would disappear if the emitter (or shunt conductance) contributions were larger than about 5%. The dominance of the base was in addition confirmed by comparing the measured dc current with that calculated from the base parameters. For $f \gtrsim 60$ kHz, the G vs f dependence for the sample in

C-2

Fig. 1 begins to bend upwards and converges to the $G \propto f^2$ dependence because of the effects of the series resistance of the sample. This range is not displayed in Fig. 1.

In the samples where the emitter contribution is small, but not negligible, $G^{HF} \propto \omega^{1/m}$, where $m < 2$ at the knee, but for higher values of ω (where the base contribution prevails) it converges to $G^{HF} \propto \omega^{1/2}$. We can then use (1) in the $\omega^{1/2}$ range to obtain

$$D_p = (1/\pi f)\,(G^{HF}/K)^2 \quad . \tag{4}$$

Using (4) for the device from Fig. 1 we obtain $\mu_p \simeq 677$ cm^2/Vs which is in very good agreement with the 608 ± 40 cm^2/Vs value obtained from (2). The latter value is more accurate because of large sensitivity of K in (4) to n_i^2 ($D_p \propto 1/K^2 \propto 1/n_i^4$). The value of n_i^2 used above was from Putley and Mitchell [20]: $n_i^2 = (9.61 \times 10^{32})T^3 \exp\,[-1206/(kT/q)]$. Note also that (4) is valid regardless of the value of S at the contact.

Table I summarizes the results from the devices used in this paper. The conductance was measured using a Wayne-Kerr B224 bridge and Hewlett-Packard 4274A and 4275A LCR meters. The device BJT is a bipolar n^+-p-n^+ transistor with a uniformly doped base with $W = 16.5$ μm and $L_n = 115$ μm [21]. The value for μ_n for this transistor was obtained from (3) by measuring the frequency dependence of i_c/v_{BE}, which is equivalent to (1) for diode. The advantage of using a bipolar transistor is that the collector current i_c always follows the ideal $\exp\,(qV_{BE}/kT)$ dependence and that the i_c depends on the base properties only. The base width W was measured using a precision mechanical indicator with a resolution of ~ 0.5 μm on the diode structures and by angle lapping and staining for the transistor. The error in W was less than about 3% for diodes

(W = 240-310 μm) and was due mostly to the nonuniformity of the large area samples used (~ 0.5-1 cm^2). This error can be reduced using smaller size samples. The dopant density was obtained by the junction C-V method. The estimated overall error of the method for the low-doped devices showing a good $G \propto f^{1/2}$ dependence is about 5%. The error will be larger for thinner high doped devices due to the increased error in determining W.

Figures 2 and 3 show the results from Table I plotted together with the results from [10] and one point from [11]. For comparison we also show the majority-carrier values by Thurber, et al. [1,2]. Our present data show that the electron minority-carrier mobility is about the same as the majority-carrier mobility, but the minority-carrier hole mobility is larger than the corresponding majority-carrier mobility. For $N_{DD} \sim 10^{15}$ cm^{-3} the difference is about 30%. Our data are thus consistent with the previous work of Dziewior and Silber [10]. Temperature dependence of μ_p and μ_n was also studied on samples from Table I in the range 300K-360K. The preliminary results are that $\mu \propto T^{-m}$, where $m \simeq 2 - 2.5$, similar to the temperature dependence of the majority- carrier mobilities [5,6].

In summary, a new method for direct measurement of the minority-carrier diffusivity and mobility was presented and demonstrated for low-doped Si. The method is accurate and requires only a knowledge of geometry in properly prepared test samples. Significant differences (~ 30%) between the minority and commonly used majority carrier values were obtained for μ_p, while μ_n was found in good agreement with the majority carrier values.

The measurements can be extended to higher concentrations up to ~ 10^{20} cm^{-3}. This however requires measurements at higher frequencies, because W has decrease as concentration increases to assure $L \gtrsim W$. Results for the concentration range 10^{19} - 10^{20} cm^{-3} will be reported separately.

ACKNOWLEDGMENTS

This work was supported by the National Science Foundation under Grant ECS-8203091, by Motorola Inc., Mesa, AZ and by JPL Contract 956525.

REFERENCES

1. W. R. Thurber, R. L. Mattis, Y. M. Liu, and J. J. Filliben, J. Electrochem. Soc., vol. 127, no. 8, p. 1807, 1980.

2. W. R. Thurber, R. L. Mattis, Y. M. Liu, and J. J. Filiben, J. Electrochem. Soc., vol. 127, no. 10, p. 2291, 1980.

3. G. Masetti, M. Severi, and S. Solmi, IEEE Trans. Electron Devices, vol. ED-30, p. 764-769, 1983.

4. J. A. del Alamo and R. M. Swanson, J. Appl. Phys., vol. 56, p. 2250, 1984.

5. S. S. Li and W. R. Thurber, Solid-State Electron., vol. 20, p. 609, 1977.

6. S. S. Li, Solid-State Electron., vol. 21, p. 1109, 1978.

7. M. B. Prince, Phys. Review, vol. 93, p. 1204, 1954.

8. F. Dannhauser, Solid-State Electron., vol. 15, p. 1371, 1972.

9. J. Krausse, Solid-State Electron., vol. 15, p. 1377, 1972.

10. J. Dziewior and D. Silber, Appl. Phys. Lett., vol. 35, p. 170, 1979.

11. D. E. Burk and V. de la Torre, IEEE Electron Device Letters, vol. EDL-5, p. 321, 1984.

12. H. S. Bennett, Solid-State Electron., vol. 26, p. 1157, 1983.

13. W. P. Dumke, Solid-State Electron, vol. 28, p. 183, 1985.

14. E. O. Kane, Solid-State Electron., vol. 28, p. 3, 1985.

15. A. Neugroschel and F. A. Lindholm, Appl. Phys. Lett., vol. 42, p. 178, 1983.

16. A. Neugroschel, F. A. Lindholm, and C. T. Sah, to be published in Solar Cells, 1985.

17. F. N. Gonzalez and A. Neugroschel, IEEE Trans. Electron Devices, vol. ED-31, p. 413, 1984.

18. A. Neugroschel, IEEE Trans. Electron Devices, vol. ED-28, p. 108, 1981.

19. T. W. Jung, F. A. Lindholm, and A. Neugroschel, IEEE Trans. Electron Devices, vol. ED-31, p. 588, 1984.

20. E. H. Putley and W. H. Mitchell, Proc. Phys. Soc. London, vol. A72, p. 193, 1958.

21. M. S. Birrittella, A. Neugroschel, and F. A. Lindholm, IEEE Trans. Electron Devices, vol. ED-26, p. 1371, 1979.

TABLE I

Summary of results at 300 K.

Device	Base Dopant	Base Doping (cm^{-3})	μ_p (cm^2/Vs)	μ_n (cm^2/Vs)
S2	Phosphorus	7.25×10^{14}	608 ± 40	
5N	Phosphorus	3.32×10^{15}	620 ± 40	
SP9	Boron	1.34×10^{15}		1288 ± 50
BJT	Boron	1.40×10^{15}		1256 ± 50
5P	Boron	6.31×10^{15}		1200 ± 100

FIGURE CAPTIONS

Fig. 1. Normalized small-signal conductance versus frequency for the sample S2 from Table I. The conductance follows the $G \propto f^{1/2}$ dependence for $f \gtrsim 25$ kHZ.

Fig. 2. Minority-and-majority-carrier hole mobilites versus doping concentration at 300 K. The error bars for the present data are also shown. The solid line is a computer curve fit of the majority-carrier data given by Thurber et al. [2]. The broken line is an approximate fit to the present and previous minority-carrier results [10].

Fig. 3. Minority-and-majority-carrier electron mobilities versus doping concentration at 300 K including error bars for the present data. A computer curve fit for majority electrons by Thurber et al. [1] is shown for comparison.

CHAPTER NINE
DISCUSSION AND RECOMMENDATION

Heavily doped polysilicon (Chapters Two and Three) provides the vehicle for a new class of silicon solar cell designs. Ultimate efficiencies may exceed 23%. This view is consistent with the projections of C. T. Sah (see Chapter Two) made in his research supported by JPL.

Our study described in Chapter Four strongly suggests the validity of the Auger-impact rate coefficients for Auger band-band recombination determined by Dziewior and Schmid (1977), despite the views of other workers. Chapter Five provides support for the model for low minority-carrier mobilities in highly doped silicon that was proposed by Neugroschel and Lindholm in 1983, under the support of JPL.

All of the issues described in Chapters Two through Five are critical both to the design of high efficiency silicon solar cells, with the aid of computer programs (such as JPL's SEEMA programs), and to the assessment of the maximum obtainable practical conversion efficiency for silicon solar cells.

Chapter Six may help prevent a misinterpretation of the connection between recombination lifetime of starting material and the photoconductive-decay data by which it is measured.

The generalized reciprocity theorem of Chapter Seven is presented in brief mathematical style. Its applications are wide, and we anticipate that many useful design results will flow from it. The connection it provides between dark current and internal quantum efficiency is outlined as a prelude to further uses.

Minority-carrier mobility and diffusivity in dilutely doped silicon has received little attention since the work of Prince in the 1950's. Appropriate values have been assumed to be available in the standard tables found in text and reference books. Our new results should be incorporated into the

numerical values used in either analytical or computer-aided design of silicon solar cell.

More important than the results of Chapter Eight is the method by which the results are obtained. An extension of this method can yield the minority-carrier diffusion coefficient and mobility of heavily doped silicon. This determination is essential for systematic design of silicon solar cells. It will lead also to a determination of the surface recombination velocity adjoining highly doped layers. The work of the Stanford group (del Alamo, Swanson, and Swirhun) supported by JPL has clarified the utility of considering the minority-carrier equilibrium concentration and the effective doping concentration as an inseparable, and experimentally determinable, quotient. This utility extends only to devices for which the heavily doped layers end at surfaces having very large surface recombination velocity S. When the surface is passivated, the minority-carrier diffusivity must be determined to yield S, and S and effective doping concentration must apparently be separately determined experimentally. Because most solar cells will have such passivation, this becomes a key issue. Furthering of the method of Chapter Eight will be part of our approach toward the solution of this design and analysis problem.

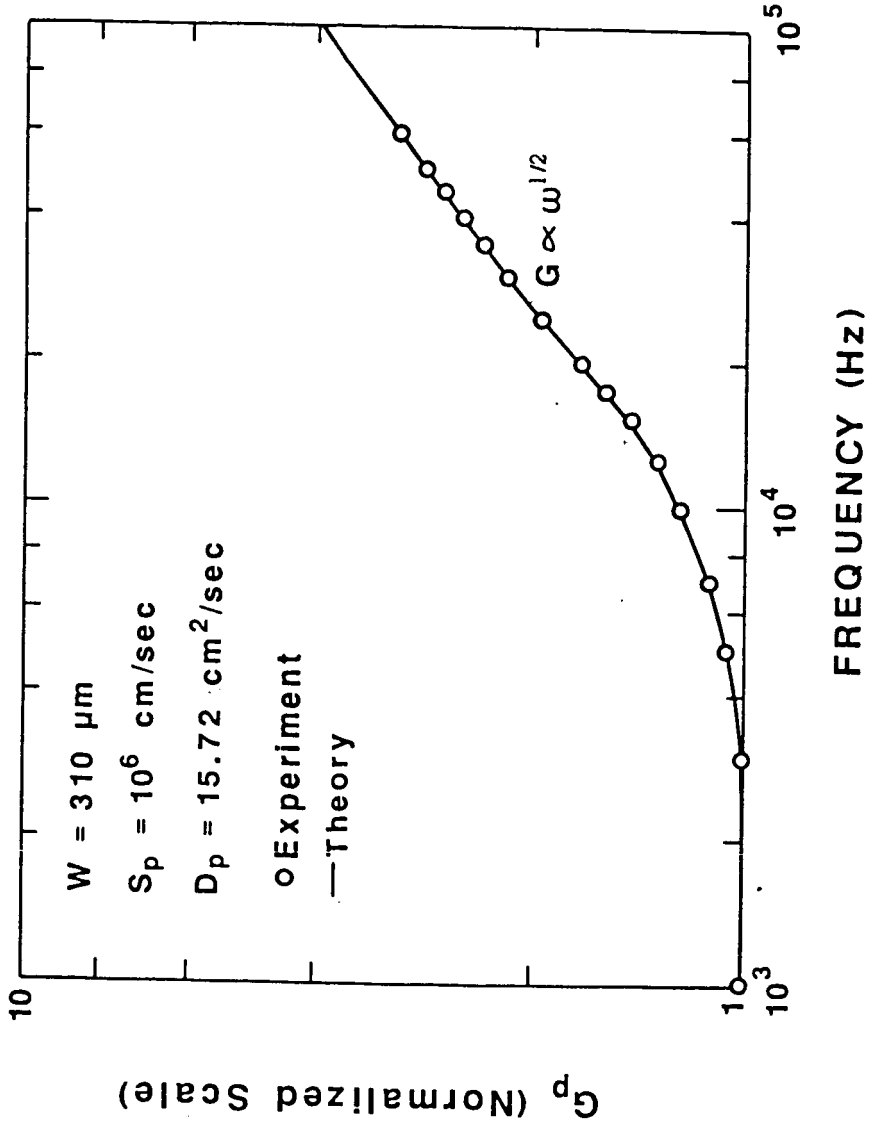
W = 310 μm
$S_p = 10^6$ cm/sec
$D_p = 15.72$ cm^2/sec
o Experiment
— Theory
$G \propto \omega^{1/2}$
10
10^3
10^4
10^5
FREQUENCY (Hz)
G_p (Normalized Scale)

FIG. 1

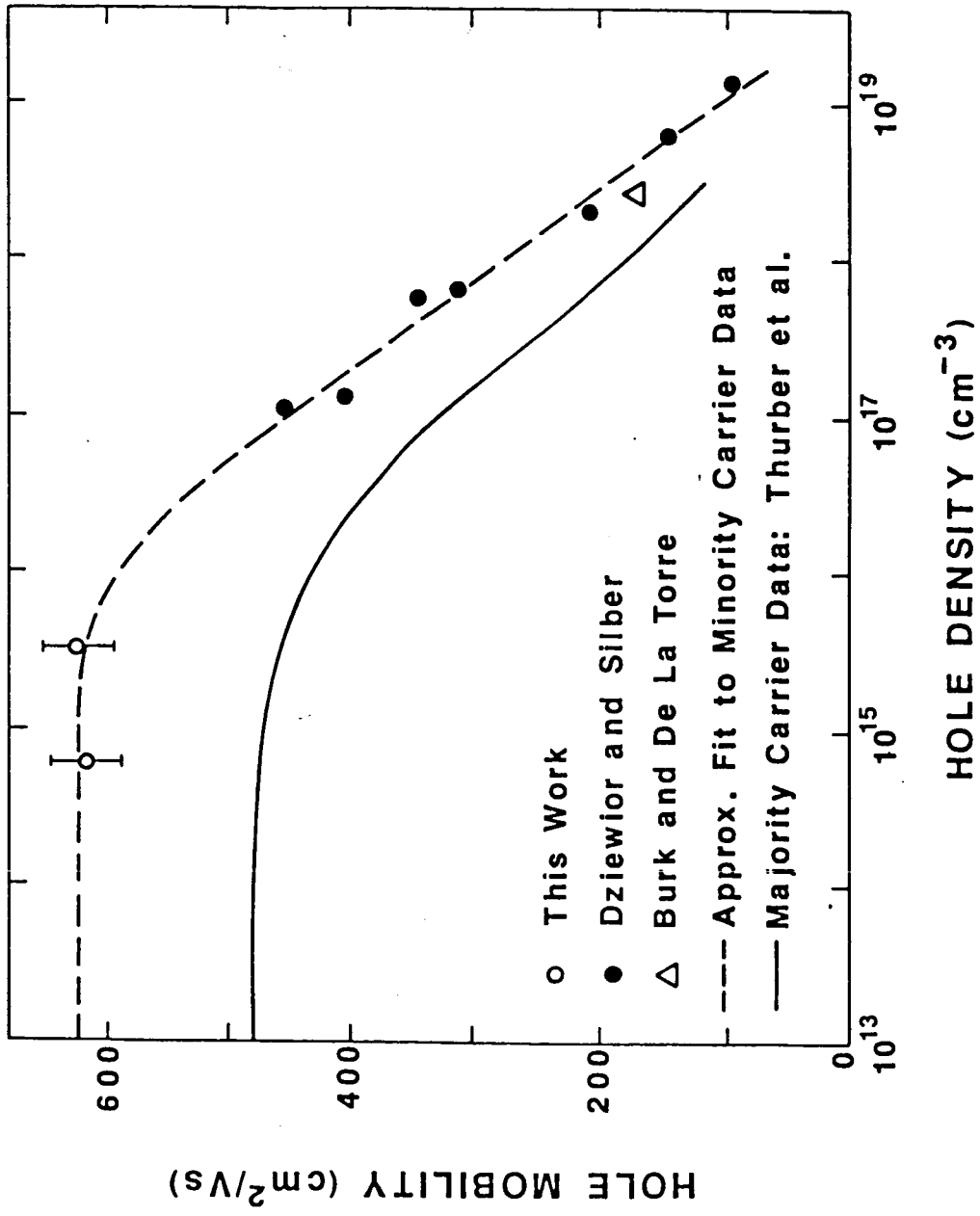
HOLE MOBILITY (cm²/Vs)
600
400
200
0
10¹³
10¹⁵
10¹⁷
10¹⁹
HOLE DENSITY (cm⁻³)
o This Work
● Dziewior and Silber
△ Burk and De La Torre
--- Approx. Fit to Minority Carrier Data
— Majority Carrier Data: Thurber et al.

FIG. 2

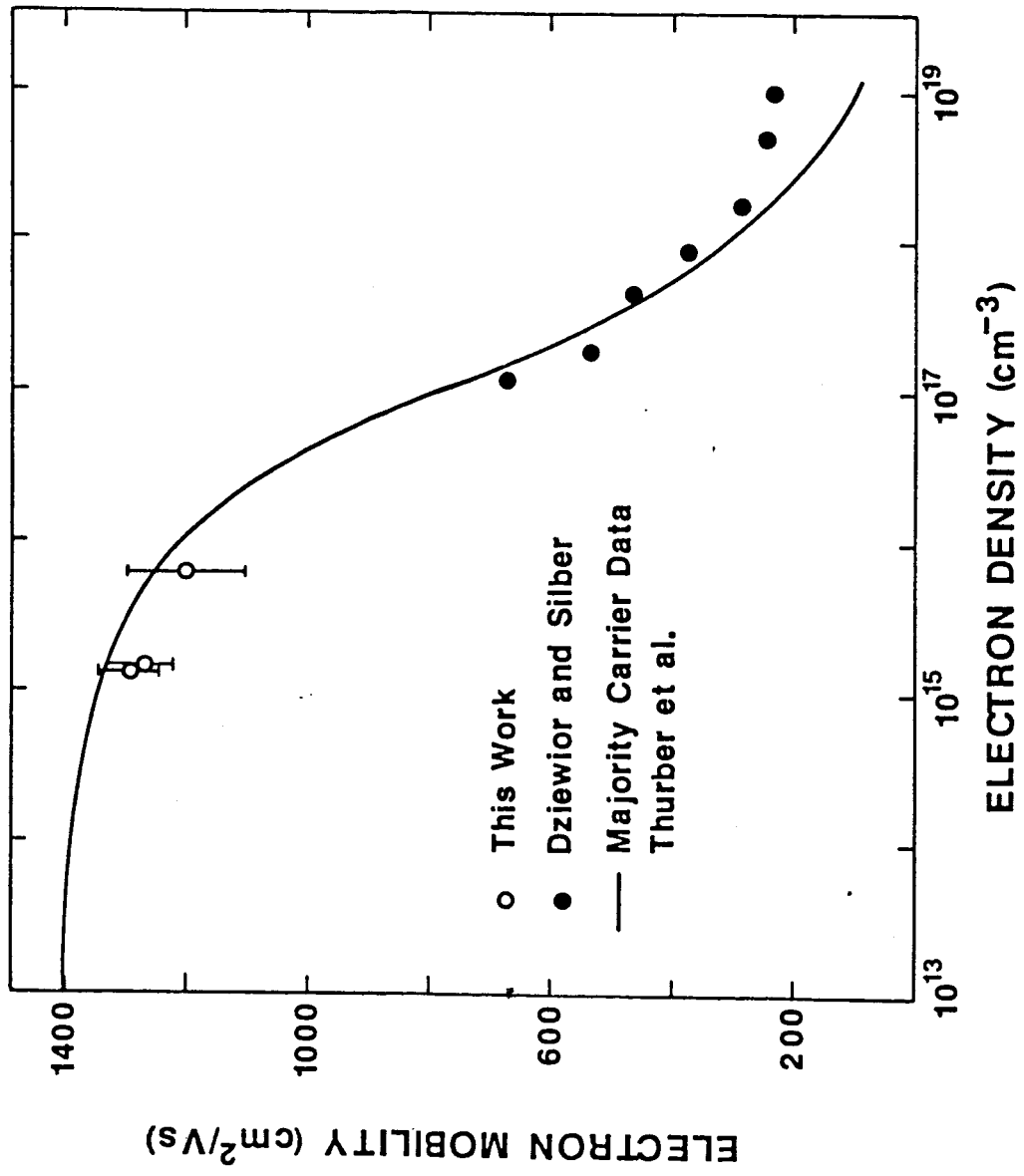
ELECTRON MOBILITY (cm²/Vs)
1400
1000
600
200
10¹³
10¹⁵
10¹⁷
10¹⁹
ELECTRON DENSITY (cm⁻³)
o This Work
● Dziewior and Silber
— Majority Carrier Data
Thurber et al.

FIG. 3